Dissertation Submitted to
Graduate School of Science of Osaka University
for the Degree of Doctor of Philosophy

Dynamics of Light Quarks and Properties of Mesons in the Multi-Instanton Vacuum of QCD

Fumiaki Araki

～2000～

Research Center for Nuclear Physics, Osaka University
10-1, Mihogaoka, Ibaraki, Osaka 567-0047, Japan

Dissertation Submitted to

Graduate School of Science of Osaka University

for the Degree of Doctor of Philosophy

Dynamics of Light Quarks and Properties of Mesons in the Multi-Instanton Vacuum of QCD

Fumiaki Araki

~ 2000 ~

Research Center for Nuclear Physics, Osaka University
10-1, Mihogaoka, Ibaraki, Osaka 567-0047, Japan

Acknowledgment

I would like to express my sincere gratitude to Professor H. Toki for stimulating collaborations and discussions and also for his continuous encouragement in my graduate course study. I would like to thank from my hart Dr. T. Watabe (Kochi Medical School) for fruitful collaborations, precious discussions and suggestions in my graduate study. He gave me thoughtful words, encouragement, manner of research and a view of the hadron physics. I am grateful to Dr. M. Fukushima for collaborations and discussions of instanton and confinement in Lattice QCD. I have enjoyed fruitful collaborations with them during my graduate course at Research Center for Nuclear Physics (RCNP), Osaka University.

I am grateful to Dr. K. Naito (RIKEN) for inviting me several times and giving me fruitful discussions and the picture of hadrons from the Nambu–Jona-Lasinio model. I would like to thank Dr. H. Suganuma (Tokyo Institute of Technology) for giving me the lecture on the topological feature in physics. I am very grateful to Professor M. Musakhanov (Tashkent State University) for guiding me to the first interest of the quark dynamics with instantons. Without their guidance, I could not find my motivation of research work.

I wish to express my appreciation to Professor A. Hosaka (Numazu College of Technology), Dr. K. Itakura (RIKEN BNL), Dr. K. Suzuki and Dr. S. Sasaki (University of Tokyo) for their passionate advice, cheerful encouragement and fruitful discussions on various physical problems. I would like to mention the warm hospitality of Dr. S. Umisedo, Dr. H. Matsufuru and Dr. N. Nakajima. They gave me valuable information for various physical subjects, computers and others. I would like to acknowledge Dr. K. Yonehara (RIKEN BNL), Dr. Y. Arimoto (SPring8) and Dr. K. Maeda for their kindness and warm friendship, and also for giving me viewpoints from experiments on physics. I would like to express my special thanks to Y. Koma, M. Takayama, T. Takahashi, S. Yasui, I. Nakamura and N. Hamamoto. Their friendship have provided me a great support on continuing my graduate course study.

Finally, I would like to thank all the members of RCNP for their kindness.

Abstract

We study the properties of SU(N_f) light quarks in the multi-instanton vacuum of QCD. The dynamical chiral symmetry breaking for light quarks of various number of flavors is formulated in several ways for multi-instanton case with specific instanton size distribution characterized by two parameters. One of them is the fall-off parameter which controls the large instanton size, and the other is the packing fraction of instantons. We get the dynamical mass of quark which depends on these two parameters and discuss its properties in detail. Such properties of the dynamical mass play relevant roles on the properties of hadrons.

For the two-flavor case, we study the properties of mesons of several channels in the quarkonium picture, by using the Bethe-Salpeter equation in the multi-instanton system with instanton size distribution. In this formalism, we extract the propagator of quarkonium of each channel and check the Goldstone mode for the pseudoscalar-triplet channel in the chiral limit. As for other mesons, we discuss two kinds of mesons in the scalar channel. Since the kernel of the Bethe-Salpeter equation is inseparable to each part of momenta of quarks incoming to it when instanton sizes are distributed widely from small sizes to large, it is difficult to proceed our remaining calculations analytically. So we calculate numerically the masses of those mesons by using the resonance fit, and then, discuss their structure.

We study also the electromagnetic properties, the electromagnetic form factor and the charge radius, for charged pions with quark-pion and the nontrivial quark-photon vertices in the multi-instanton background in the flavor SU(2) framework. The quark-pion vertex is obtained from the Bethe-Salpeter amplitude with the instanton kernel. For the quark-photon vertex, on the other hand, we provide the correction term which is made of the quark dynamical mass in the instanton background and satisfied with the Ward-Takahashi identity. Although all of our calculations are made in off-shell states of pions, we discuss also their justification for the on-mass-shell limit of pions. From this approach, we obtain a reasonable value of the pion charge radius without the assumption of the vector meson dominance.

Contents

List of Figures

Chapter 1

Introduction

1.1 Mesons and nonperturbative feature of QCD

Nowadays, quantum chromodynamics (QCD) is widely accepted to be the underlying theory of the strong interaction, with quarks and gluons as fundamental degrees of freedom. In the perturbative regime, i. e. at short distances which are probed with high momentum transfer phenomena, QCD results within perturbation theory agree quantitatively with the experimental data. On the other hand, it has been impossible for us to derive analytically detailed descriptions of large distance phenomena from QCD Lagrangian at the present.

Mesons seem to be the ideal systems for the study of strong interaction in the nonperturbative region, which are unsolvable from QCD Lagrangian. In order to describe such meson properties, many alternative models and frameworks have been proposed. One of the most successful scheme is the quarkonium picture, where a quark and an anti-quark form a color singlet bound state. This picture perfectly describes the mass spectra of the lowest lying resonances in the pseudoscalar channel, so-called pseudoscalar nonet, where π, K, η and η' are involved [1].

On the other hand, the lattice gauge theory predicts another type of mesons with explicit glue degrees of freedom. These are the glueballs, which have no valence quark. Calculations based on the lattice gauge theory suggest that the lightest glueball is a scalar resonance ($J^{PC} = 0^{++}$) with a mass of 1600±150 MeV [2, 3]. Around 1600 MeV in isoscalar-scalar channel there exist two established resonances. One of them is $f_0(1710)$ and the other is $f_0(1500)$. It is natural to expect a mixing between the scalar quarkonium state and the lightest scalar glueball. These states are so-called hybrids. Lee and Weingarten evaluated the mixing energy between the scalar quarkonium state and the lightest scalar glueball [4]. Their results support the interpretation of $f_0(1710)$ as composed mainly of the lightest scalar glueball.

Below 1 GeV the mass spectra in the scalar channel show another feature. On the $K\bar{K}$ threshold there are two resonances. One is the isoscalar resonance, $f_0(980)$, and the other is isotriplet, $a_0(980)$. Weinstein and Isgur studied the $K\bar{K}$ molecule interpretation of these two states. [5] They show that the $K\bar{K}$ molecules have properties consistent with experimental results on the production of $f_0(980)$ and $a_0(980)$ and of low-mass $K\bar{K}$ pairs. The $K\bar{K}$ molecule interpretation of the two states on the $K\bar{K}$ threshold is supported also by the calculations based on the chiral unitary approach in the chiral perturbation framework [6]. In Ref. [6] the phase shifts for $\pi\pi \to \pi\pi$ as a function of the c.m. energy of the meson pair in the various channels are well reproduced and in a good agreement with experiments. In the isoscalar-scalar channel, $f_0(400-1200)$, which is often referred as σ, is also reproduced. Hence, in a sense, the broad $f_0(400-1200)$ should be understood as the $\pi\pi$ and $K\bar{K}$ resonances. However, on the other hand, Ishida reanalyzed the $\pi\pi$- and $K\pi$-scattering phase shifts and reported an observation on $\sigma(600)$-particle in the isoscalar-scalar channel [7].

In the chiral quark theory like the Nambu–Jona-Lasinio model, the σ meson appears as a quarkonium with a mass of 600-700 MeV [8]. It is the chiral partner of the π meson, which is the Goldstone boson in the theory. In general, it is quite natural to consider the σ meson

as the chiral partner of the π meson, existing with a mass around 700 MeV. However the resonance around 700 MeV in the isoscalar-scalar channel, $f_0(400-1200)$, has a very broad structure with a width of 600-1000 MeV. Hence the interpretation of $f_0(400-1200)$ in terms of a quarkonium still remains open.

1.2 QCD vacuum and instantons

As we have seen above, there are many kinds of effective model which can describe well the meson spectra. On the other hand, it is expected that the structure of mesons, and furthermore hadrons, should be understood starting from the structure of the QCD vacuum. Since hadrons are collective excitations, we can not ignore the properties of the ground state when we study its excitations. For the QCD vacuum and its nonperturbative nature, many kinds of model had been proposed. Most of the attempts to describe the QCD ground state were based on the idea that the vacuum is dominated by the classical configuration of gauge fields. It was found that the use of instantons reproduces some important aspects of nonperturbative phenomena of QCD. An instanton is a solution of the Euclidean Yang-Mills equation, which was first discovered by Polyakov and coworkers [9] motivated by the search for classical solutions with nontrivial topology in analogy with the 't Hooft-Polyakov monopole [10]. Thereafter, a number of authors clarified the physical meaning of the instanton as a tunneling event between degenerate classical vacua [11–13]. These works also introduced the concept of θ-vacua in connection with QCD.

An important development was made by 't Hooft [14], who calculated the semi-classical tunneling rate of instanton vacua. In this context, he discovered the presence of zero modes in the spectrum of the Dirac operator. This result implied that tunneling is intimately connected with light fermions, in particular that every instanton absorbs one left handed fermion of every species, and emits a right handed one (and vice versa for anti-instantons).

This result also explained how anomalies are related to instantons, for example the violation of axial charge in QCD and baryon number in electroweak theory.

A particular instanton-induced effect, the anomalous breaking of $U(1)_A$ symmetry and the η' mass, deserves special attention. Witten and Veneziano wrote down an approximate relation that connects the η' mass with the topological susceptibility [15,16]. This was a very important step, since it was the first quantitative result concerning the effect of the anomaly on the η' mass.

1.3 Phenomenological approaches

Although instantons enable us to provide good explanations of QCD vacuum and the anomalous profile of η' meson, there is no experimental evidence for instanton effects, and no theoretical control over semi-classical methods in QCD. In order to find a way to go further, several phenomenological approaches to the structure of the QCD vacuum were studied. One of the greatest progress for studying instanton phenomenology was brought by the instanton liquid model [17] proposed by Shuryak. This model suggests the two basic parameters of the instanton ensemble, the mean density of instantons $n \simeq 1$ fm^{-4} and their average size $\rho \simeq 1/3$ fm. This means that the space-time volume occupied by instantons $n\rho^4$ is small, that is, the instanton ensemble is dilute. Using these instanton liquid parameters, the phenomenological values of the quark and gluon condensates are reproduced. In addition, one can calculate direct instanton corrections to hadronic correlation functions at short distance. The results were found to be in good agreement with experiment in pseudo-scalar meson channels [18]. Theoretical justification for the instanton liquid model was taken by using the variational techniques and the mean field approximation to deal with the statistical mechanics of the instanton liquid [19,20]. The resulting ensembles were found to be consistent with the phenomenological estimates.

The instanton ensemble in the presence of light quarks was studied by Diakonov and Petrov [21]. This work introduced the picture of the quark condensate as a collective state built from delocalized zero modes. The quark condensate was calculated using the mean field approximation and found to be in agreement with experiment.

1.4 Instantons and confinement

As expressed so far, the use of instantons seems to be a reasonable choice for nonperturbative treatment of QCD phenomena. If the instanton ensemble is appropriate to the QCD vacuum, color confinement, the character that all colored particles are not isolated each other but always observed as color-singlet states, is also to be explained from the context of instantons. The early concept of instanton received much attention due to Polyakov's discovery that instantons cause confinement in certain 3-dimensional models [13]. However, several studies of instantons in those days gave a negative result on confinement.

Recent development of both theoretical and numerical approaches for confinement have indicated a new viewpoint of instantons. It is theoretically well-known that condensation of the color-magnetic monopole causes confinement in the context of the dual representation of the superconductivity [22–30]. In the lattice QCD, a picture of monopole condensation is represented to relatively long monopole loops, closed monopole world-lines in 4-dimension. The topologically nontrivial linkage between monopoles and instantons was found in specific gauge choices theoretically [31,32] and numerically [33–37]. This suggests that the instanton ensemble may contribute to the monopole condensation. At the same time, the treatment of large size instantons were important steps. It was found that falling off of large size by the power law leads to the confining potential in the heavy quark theory [38,39]. Several lattice simulations indicated the same law [40,41].

Thus, it seems to be more realistic that the instanton ensemble with size distribution falling

off by the power law in the large size region is considered for confinement. Based on above, we will study the structure of mesons as quark-antiquark bound state in the multi-instanton background with the size distribution.

In Sect. 2, we will follow relations between quark zero-modes and the instanton ensemble using the variational principle [21] with specific size distribution. It will be shown that the chiral symmetry is broken dynamically and a current quark in the chiral limit carries a mass originated in the instanton kernel. Simultaneously, the contribution of the size distribution of instantons will be discussed. In Sect. 3, we will study a quarkonium with instanton media by using the Bethe-Salpeter formalism. It will be considered *the propagator* of the pseudoscalar-isotriplet channel in the chiral limit and shown that it is surely the Goldstone mode. In addition, the scalar channel will be also considered and discussed the value of mass naively. In Sect. 4, We will restrict ourselves to the pseudoscalar isotriplet channel which we recognize it as the pion, and study its electromagnetic property, the electromagnetic form factor, in the space-like Q^2 region, where Q^2 is a squared incoming momentum of photon. This calculation is performed in the off-shell kinematics. However, when $Q^2 = 0$, it is available to discuss the on-shell pion because of masslessness in the chiral limit. Furthermore, we will derive and discuss the pion charge radius in the instanton background with size distribution of instantons. We will include the nontrivial quark-photon vertex since a photon couples with a quark which carries the dynamical mass. Final section is devoted to the summary and conclusion.

Chapter 2

Effective fermion action in the instanton background

First of all, we briefly review the formalism of instantons. We shall discuss the behavior of quarks in the instanton background.

2.1 Instanton as QCD vacuum

Historically instantons were found as topologically nontrivial solutions of the duality equations of the Euclidean Yang-Mills theory [9]. To find these solutions, it is convenient to exploit the following identity

$$\begin{aligned} S &= \frac{1}{4g^2}\int d^4x\, G^a_{\mu\nu}G^a_{\mu\nu} \quad \left(= \frac{1}{4g^2}\int d^4x\, \tilde{G}^a_{\mu\nu}\tilde{G}^a_{\mu\nu}\right) \\ &= \frac{1}{4g^2}\int d^4x \left[\pm G^a_{\mu\nu}\tilde{G}^a_{\mu\nu} + \frac{1}{2}\left(G^a_{\mu\nu} \mp \tilde{G}^a_{\mu\nu}\right)^2\right], \end{aligned} \tag{2.1}$$

where $G^a_{\mu\nu}$ is the field strength tensor of the SU(2) gauge field. $\tilde{G}^a_{\mu\nu} = 1/2\epsilon_{\mu\nu\rho\sigma}G^a_{\rho\sigma}$ is the dual field strength (the field tensor in which the roles of electric and magnetic fields are

interchanged). Since the last term is always positive, it is clear that the action is minimal if the field is (anti) self-dual

$$G^a_{\mu\nu} = \pm\tilde{G}^a_{\mu\nu} \quad . \tag{2.2}$$

The action of a self-dual field configuration is written by the so-called topological charge (or 4 dimensional Pontryagin index)

$$Q = \frac{1}{32\pi^2}\int d^4x\, G^a_{\mu\nu}\tilde{G}^a_{\mu\nu} \tag{2.3}$$

From (2.1), we have $S = (8\pi^2|Q|)/g^2$ for self-dual fields. For finite action field configurations, Q has to be an integer. This can be seen from the fact that the integrand is a total derivative

$$Q = \frac{1}{32\pi^2}\int d^4x\, G^a_{\mu\nu}\tilde{G}^a_{\mu\nu} = \int d^4x\, \partial_\mu K_\mu = \int_{S^3} d\sigma_\mu K_\mu, \tag{2.4}$$

$$K_\mu = \frac{1}{16\pi^2}\epsilon_{\mu\alpha\beta\gamma}\left(A^a_\alpha\partial_\beta A^a_\gamma + \frac{1}{3}f^{abc}A^a_\alpha A^b_\beta A^c_\gamma\right) \quad . \tag{2.5}$$

For finite action configurations, the gauge field has to be pure gauge form at infinity,

$$A_\mu(x) \longrightarrow iU(x)\partial_\mu U^\dagger(x) \quad , \tag{2.6}$$

where $U(x) \in \mathrm{SU}(2)$ and $A_\mu := A^a_\mu T^a$ with T^a being the Lie algebra of SU(2). Inserting $A_\mu = iU\partial_\mu U^\dagger$ into Eq. (2.4), one can find that Q represents the winding number which classifies the mapping from the sphere S^3 (corresponding to spacial infinity) into the gauge group SU(2).

Furthermore, if the gauge field falls off sufficiently rapidly at spatial infinity,

$$Q = \int dt\frac{d}{dt}\int d^3x K_0 = n_{CS}(t=\infty) - n_{CS}(t=-\infty) \tag{2.7}$$

which shows that field configurations with $Q \neq 0$ connect different topological vacua. Let us find an explicit solution with $Q = 1$. We can take $A_\mu = iU\partial_\mu U^\dagger$ with $U = i\hat{x}_\mu\tau^+_\mu$, where $\tau^\pm_\mu = (\vec{\tau}, \mp i)$. Then $A^a_\mu = 2\eta_{a\mu\nu}x_\nu/x^2$, where we have introduced the 't Hooft symbol $\eta_{a\mu\nu}$.

It is defined by

$$\eta_{a\mu\nu} = \begin{cases} \epsilon_{a\mu\nu} & \mu, \nu = 1, 2, 3 \quad , \\ \delta_{a\mu} & \nu = 4 \quad , \\ -\delta_{a\nu} & \mu = 4 \quad , \end{cases} \tag{2.8}$$

and self-dual in the vector indices (see also Appendix A.1). We also define the anti-self-dual tensor, $\overline{\eta}_{a\mu\nu}$, by changing the sign of the last two equations. We can now look for a solution of the self-duality equation (2.2) using the ansatz $A^a_\mu = 2\eta_{a\mu\nu}x_\nu f(x^2)/x^2$, where $f(x^2)$ has to satisfy the boundary condition $f \to 1$ as $x^2 \to \infty$. Inserting the ansatz in Eq. (2.2), we get

$$f(1-f) - x^2 f' = 0. \tag{2.9}$$

This equation is solved by $f = x^2/(x^2+\rho^2)$, which gives the BPST instanton solution [9]

$$A^a_\mu(x) = \frac{2\eta_{a\mu\nu}x_\nu}{x^2+\rho^2}. \tag{2.10}$$

Here ρ is an arbitrary parameter characterizing the size of the instanton. A solution with topological charge $Q = -1$ can be obtained by replacing $\eta_{a\mu\nu} \to \overline{\eta}_{a\mu\nu}$. The corresponding field strength is

$$G^a_{\mu\nu} = -\frac{4\rho^2\eta_{a\mu\nu}}{(x^2+\rho^2)^2} \quad . \tag{2.11}$$

In our conventions, the coupling constant only appears as a factor in front of the action. This convention is very convenient in dealing with classical solutions. For perturbative calculations, it is more common to rescale the fields as $A_\mu \to gA_\mu$. In this case, there is a factor $1/g$ in the instanton gauge field, which shows that the field of the instanton is much stronger than ordinary, perturbative, fields.

Also note that $G^a_{\mu\nu}$ is well localized (it falls off as $1/x^4$) despite the fact that the gauge field is long-range, $A_\mu \sim 1/x$. The invariance of the Yang-Mills equations under coordinate inversion [11] implies that the singularity of the gauge field can be shifted from infinity to the origin by means of a (singular) gauge transformation $U = i\hat{x}_\mu\tau^+_\mu$. The gauge field in singular

gauge is given by

$$A^a_\mu(x) = 2\frac{x_\nu}{x^2}\frac{\overline{\eta}_{a\mu\nu}\rho^2}{x^2+\rho^2} \quad , \tag{2.12}$$

and the field strength is

$$G^a_{\mu\nu} = -\frac{4\rho^2}{(x^2+\rho^2)^2}\left(\bar{\eta}_{a\mu\nu} - 2\bar{\eta}_{a\mu\alpha}\frac{x_\alpha x_\nu}{x^2} - 2\bar{\eta}_{a\alpha\nu}\frac{x_\alpha x_\mu}{x^2}\right) \quad . \tag{2.13}$$

This singularity at the origin is not physical, the field strength and topological charge density are smooth. However, in order to calculate the topological charge from a surface integral over K_μ, the origin has to be surrounded by a small sphere. The topology of this configuration is therefore located at the origin, not at infinity. In order to study instanton-anti-instanton configurations, we will mainly work with such singular configurations.

The classical instanton solution has a number of degrees of freedom, known as collective coordinates. In the case of $N_c = 2$, the solution is characterized by the instanton size ρ, the instanton position z_μ, and three parameters which determine the color orientation of the instanton. The group orientation can be specified in terms of the SU(2) matrix U, $A_\mu \to UA_\mu U^\dagger$, or the corresponding rotation matrix $R^{ab} = \frac{1}{2}\mathrm{tr}(U\tau^a U^\dagger \tau^b)$, such that $A^a_\mu \to R^{ab}A^b_\mu$. Due to the symmetries of the instanton configuration, ordinary rotations do not generate new solutions.

In case of $N_c = 3$ instantons can be constructed by embedding the SU(2) solution. For $|Q| = 1$, there are no genuine SU(3) solutions. The number of parameters characterizing the color orientation is seven, not eight, because one of the SU(3) generators leaves the instanton invariant. For SU(N_c), the number of collective coordinates (including position and size) is $4N_c$.

There exist exact n-instanton solutions with $4nN_c$ parameters, but they are difficult to construct in general [42]. A simple solution where the relative color orientations are fixed

was given by 't Hoof [43, 44]. His starting point is as follows. Let us assume that

$$A^a_\mu = \frac{1}{g}\eta_{a\mu\nu}\partial_\nu\phi \quad , \tag{2.14}$$

where ϕ is a scalar function of x and collective coordinates. It is rather easy to show that within this ansatz the duality condition for the field strength tensor results in an equation on ϕ which essentially reduces to that on the scalar potential in electrostatics,

$$\frac{1}{\phi}\partial^2\phi = 0 \quad . \tag{2.15}$$

The solution of Eq. (2.15) is given by a sum of four-dimensional Coulomb potentials from point-like sources arbitrarily located in four-dimensional space,

$$\phi = 1 + \sum_{i=1}^{n} \frac{\rho_i^2}{(x - y_i)^2} \quad . \tag{2.16}$$

The resulting field configuration describes n instantons in the singular gauge, with arbitrary positions and all with one and the same orientation in the color space.

In the rest of this paper, we will not use the multi-instanton solution, Eq. (2.16), as we can not consider the degree of freedom of color orientations of each instanton. Instead of Eq. (2.16), we will use *the sum Ansatz* in which we sum up all individual instanton configurations in getting the multi-instanton configuration. Concerning this ansatz, we will give further information in section 2.3.

2.2 Quark zero-mode and instanton

The quark sector is an important part of QCD. Although the existence of instantons is due to the nontrivial topology of the gauge fields, it leads to a drastic effect on the fermion fields [14]. The point is that instantons make explicit the nonconservation of certain fermion numbers associated with the anomaly in the axial current.

The nonconservation of the axial current indicates a disproportion between the number of the left-handed field and the right. Actually, we can find the fact by decomposing the quark field ψ into the left-handed and right-handed fields, ψ^L and ψ^R, respectively. In the absence of the mass term, the two fields decouple from each other in the Lagrangian,

$$\mathcal{L} = \bar{\psi} i \not{D} \psi = \bar{\psi}^L i \not{D} \psi^L + \bar{\psi}^R i \not{D} \psi^R \quad . \tag{2.17}$$

Here, we have omitted flavor indices of quarks for simplicity. Hence, Feynman graphs of any order conserves separately the number of each of chiral fields, n_L and n_R. It means that the Lagrangian possesses two conserved charges, q and q_5, associated with the vector current $j^\mu := \bar{\psi}\gamma^\mu\psi$ and the axial current $j_5^\mu := \bar{\psi}\gamma^\mu\gamma^5\psi$, respectively. The first charge counts the total number of chiral fields, $q = n_L + n_R$, while the second one counts the difference, $q_5 = n_L - n_R$. Classically, the underlying U(1) symmetry leads to the conservation of the vector current and electric charge, $\partial_\mu j^\mu = 0$ and $\dot{q} = 0$. Similarly, the axial $\mathrm{U_A}(1)$ symmetry implies the conservation of the axial current and the axial charge, $\partial_\mu j_5^\mu = 0$ and $\dot{q}_5 = 0$, in the absence of mass term. However, the axial current is actually anomalous [?, ?] as

$$\partial_\mu j_5^\mu = \frac{1}{16\pi^2} G^a_{\mu\nu} \widetilde{G}^a_{\mu\nu} \quad . \tag{2.18}$$

The right hand side is a total derivative, $G^a_{\mu\nu}\widetilde{G}^a_{\mu\nu} \propto \partial_\mu K_\mu$, where K_μ is the Charn-Simons current defined in Eq. (2.5). As we previously mentioned, the surface integral of K_μ gives an integer, $Q \neq 0$, for the instanton configuration, while this integral is zero for trivial gauge configuration. Thus, the conservation of q_5 is lost in the instanton background. Hence, instantons are relevant for the anomalous divergence of axial current and expected to solve the $\mathrm{U_A}(1)$ problem in QCD.

The crucial property of instantons is that the Euclidean Dirac operator has a zero mode, that is, $i\not{D}\psi_0 = 0$ in the instanton configuration [14]. The solution of this equation is shown as follows. We observe that

$$(i\not{D})^2 = -D^2 + \frac{1}{2}\sigma_{\mu\nu} G_{\mu\nu} \quad . \tag{2.19}$$

When the field strength is (anti-)self-dual, it satisfies $(1 \pm \gamma_5)\sigma_{\mu\nu}G^{(\pm)}_{\mu\nu} = 0$, where the plus sign denotes self-dual and the minus anti-self-dual. Then, in case of the self-dual field in the singular gauge, the zero mode Dirac equation implies

$$\left(-D^2 + \frac{1}{2}\sigma_{\mu\nu}G^{(+)}_{\mu\nu}\right)\psi^L_0 = 0 \qquad \text{and} \qquad -D^2\psi^R_0 = 0 \quad , \tag{2.20}$$

with $\psi_0 = \psi^L_0 + \psi^R_0$, and vice versa ($+ \leftrightarrow -$, $L \leftrightarrow R$) for anti-self-dual. Since $-D^2 = (iD)^2$ is a positive operator because of iD being Hermitian, ψ^R_0 has to vanish and the zero mode in the background of an instanton has to be left-handed, while it is right-handed in the case of an anti-instanton. Solving Eq. (2.20) for an instanton in the singular gauge, we get

$$\psi^{\beta n}_0(x) = \phi(x,\rho)\left[\not{x}\frac{1+\gamma_5}{2}\right]^{nm} U^{\beta\alpha}\chi^{\alpha m} \quad , \tag{2.21}$$

$$\phi(x,\rho) := \frac{\rho}{\pi}\frac{1}{\sqrt{x^2}(x^2+\rho^2)^{3/2}} \quad , \tag{2.22}$$

with the extra color matrix U. Here, $\chi^{\alpha m} := (u^{\alpha m}, u^{\alpha(m-2)})^T$ and u is a constant 2-spinor in which the SU(2) color indices, α and β, is coupled to the spin indices, $m, n = 1, 2$. The constant spinor u is antisymmetric for color and spin indices as $u^{\alpha m} = \epsilon^{\alpha m}/\sqrt{2}$. In case of the anti-self-dual field, we can get the solution by changing $\frac{1}{2}(1+\gamma_5)$ to $\frac{1}{2}(1-\gamma_5)$.

Thus, it is found that quarks are affected by instantons through the left- or right-handed zero-modes of quarks. The number of the fermion zero modes is related to the topological charge of instantons by the Atiyah-Singer index theorem [45] that requires that $q_5 = n_L - n_R$ for every species of chiral fermions. In the case of instantons, this relation was proved by Schwartz [46].

2.3 Fermion determinant

We study the behaviors of the light quarks in the multi-instanton vacuum of QCD The QCD vacuum is assumed as an ensemble of instantons and anti-instantons. Diakonov et

al. developed an effective theory for light quarks based on the multi-instanton vacuum of QCD [21, 47]. In this section, we will review the work for further development.

To make the effective fermion action, we try to get the fermion propagator. In the background of the multi-instanton configuration, the Dirac operator is given as

$$D_\mu = \partial_\mu - iA_\mu(x;\xi) \quad , \tag{2.23}$$

with the instantons in *the sum ansatz*,

$$A(x;\xi) = \sum_{I}^{N_+} A_+(x;\xi_I) + \sum_{\bar{I}}^{N_-} A_-(x;\xi_I) \quad . \tag{2.24}$$

where $A_\pm$ are the fields of individual instantons (I's) and anti-instantons ($\bar{I}'s$) in the singular gauge [11]. The symbols ξ_I and $\xi_{\bar{I}}$ denote the set of collective coordinates of the Ith instanton and $\bar{I}$th anti-instanton, respectively. In the presence of a single instanton, the fermion propagator has a singularity in the chiral limit due to the zero mode [48]. The authors of Ref. [47] approximate it as the sum of the free propagator and the explicit contribution of the zero mode,

$$(-i\not{D} + m_f)^{-1}_{1-\text{inst}} \approx (-i\not{\partial})^{-1} + \frac{\psi_0(x;\xi_{I(\bar{I})})\psi_0^\dagger(x;\xi_{I(\bar{I})})}{m_f} \quad , \tag{2.25}$$

where $\psi_0(x;\xi_{I(\bar{I})})$ are the wave functions of the fermion zero mode in the background of one (anti-)instanton with the collective coordinates $\xi_{I(\bar{I})} = (z_{I(\bar{I})}, U_{I(\bar{I})}, \rho_{I(\bar{I})})$. The idea of the approximation, Eq. (2.25), is based on the eigenstate representation of the fermion Dirac operator. When we explicitly write down the propagator in terms of quark mass m_f, the first term of r.h.s should be written as

$$\sum_{n\neq 0} \frac{\psi_n(x)\bar{\psi}_n(x)}{\lambda_n + m_f} \quad , \tag{2.26}$$

In the chiral limit, $m_f \to 0$, the second term of the r.h.s. of Eq. (2.25) dominates around the instanton. Hence, the authors of Ref. [47] simply replace it with the free propagator as a good approximation.

Eq. (2.25) is equivalent to using an approximate action [49],

$$\exp\left(-\widetilde{S}^{I(\bar{I})}[\bar{\psi},\psi]\right) \propto \exp\left(-\sum_f^{N_f}\int d^4x\bar{\psi}_f(-i\partial\!\!\!/)\psi_f\right)\prod_f^{N_f}\left(1+\frac{1}{m_f}V_\pm^{I(\bar{I})}[\bar{\psi}_f,\psi_f]\right) \quad , \quad (2.27)$$

with

$$V_\pm^{I(\bar{I})}[\bar{\psi}_f,\psi_f] = \int d^4x\left(\bar{\psi}_f(x)(-i\partial\!\!\!/_x)\psi_{0,\pm}(x;\xi_{I(\bar{I})})\right)\int d^4y\left(\psi^\dagger_{0,\pm}(y;\xi_{I(\bar{I})})(-i\partial\!\!\!/_y)\psi_f(y)\right) \quad . \quad (2.28)$$

We obtain the expression, Eq. (2.25), for the quark propagator following the standard procedure of getting the propagator from this action.

Assuming the diluteness of the instanton medium, we obtain the fermion action in the background of a multi-instanton configuration by the product of contributions from each flavor and (anti-)instanton. Then the averaged fermion determinant is obtained as

$$\begin{aligned}\overline{\mathrm{Det}}_{N_\pm} &= \int \mathcal{D}\bar{\psi}\mathcal{D}\psi\int\prod_I^{N_+ + N_-}\frac{d^4z_I}{V}dU_I d\rho_I f(\rho_I)\exp\left(-\tilde{S}[\bar{\psi},\psi]\right)\\ &= \int \mathcal{D}\bar{\psi}\mathcal{D}\psi\exp\left(-\sum_f^{N_f}\int d^4x\bar{\psi}_f(-i\partial\!\!\!/)\psi_f\right)W_+^{N_+}W_-^{N_-} \quad , \end{aligned} \quad (2.29)$$

where $W_\pm$ denote the single-instanton averages,

$$W_\pm[\bar{\psi},\psi] = \int\frac{d^4z_{I(\bar{I})}}{V}dU_{I(\bar{I})}d\rho_{I(\bar{I})}f(\rho_{I(\bar{I})})\prod_f^{N_f}\left(1+\frac{1}{m}V_\pm^{I(\bar{I})}[\bar{\psi}_f,\psi_f]\right) \quad . \quad (2.30)$$

with $m_1 = m_2 = \cdots = m_{N_f} = m$ due to the flavor symmetry. We have formally written the instanton distribution function as $f(\rho_I)$. The instanton sizes, ρ_I, are unknown parameters which are valued from zero to infinity. The integration over instanton size is troublesome with respect to the divergence in the infrared domain [48]. We will discuss the suitable instanton size distribution in the next section.

To proceed, we expand the N_f products (the bracket) in Eq. (2.30) and get a series of terms characterized by the power of $1/m$. Then we perform the integration over the color space rotation variables, $\int dU_{I(\bar{I})}$ (see Appendix A.2), to leading order in $1/N_c$ on each term of order

$\mathcal{O}(1/m^{N_f})$. For instance, one of the terms of order $\mathcal{O}(1/m^{N_f})$ consists of $\prod_{f=1}^{N_f} V_{\pm}^{I(\bar{I})}[\bar{\psi}_f, \psi_f]$, and for this term the integral over the color space rotation variables leads,

$$\frac{1}{m^{N_f}} \int dU_{I(\bar{I})} \prod_{f=1}^{N_f} V_{\pm}^{I(\bar{I})}[\psi_f, \psi_f] = \det{}_{fg} J_{\pm fg}(z_{I(\bar{I})}, \rho_{I(\bar{I})}), \tag{2.31}$$

where the currents, $J_{\pm}(z, \rho)$, are color singlets and $N_f \times N_f$ matrices in flavor,

$$J_{\pm fg}(z, \rho) = -\frac{4\pi^2 \bar{\rho}^2}{m N_c} \int \frac{d^4k}{(2\pi)^4} \frac{d^4l}{(2\pi)^4} e^{-i(k-l)\cdot z} \left(\frac{\rho}{\bar{\rho}}\right)^2 F(|k|\rho) F(|l|\rho) \left\{ \bar{\psi}_f(k) \frac{1 \mp \gamma^5}{2} \psi_g(l) \right\} \quad . \tag{2.32}$$

In Eq. (2.31) the notation $\det_{fg}$ means a determinant of the matrix $J_{\pm}$ in the flavor space. $F(|k|\rho)$ in Eq. (2.32) is a function originating from the wave function of the zero mode in momentum space,

$$2\pi\rho \frac{\not{k}}{|k|^2} F(|k|\rho) = \int d^4x \; e^{ik\cdot x} i\not{\phi}(x, \rho) \quad . \tag{2.33}$$

The explicit form of $F(|k|\rho)$ is given as

$$F(|k|\rho) = 2\left\{ t\Big(I_0(t)K_1(t) - I_1(t)K_0(t) \Big) - I_1(t)K_1(t) \right\} \quad \text{with} \quad t = \frac{1}{2}|k|\rho \quad , \tag{2.34}$$

where I and K are modified Bessel functions of the first and second kinds, respectively. The single-instanton averages, Eq. (2.30), are finally expressed as [47]

$$W_{\pm} = \int \frac{d^4z}{V} d\rho f(\rho) \det\Big[J_{\pm}(z, \rho) + 1 \Big] \quad , \tag{2.35}$$

where the determinant is over flavor indices and the current, $J_{\pm}(z, \rho)$ are $N_f \times N_f$ matrices in the flavor space.

We note the meaning of the large N_c limit, $N_c \to \infty$, and the chiral limit, $m \to 0$, in the evaluation of $\det[J_{\pm}(z, \rho)+1]$ in Eq.(2.35). Since the currents, $J_{\pm}(z, \rho)$, are proportional to the factor $1/(mN_c)$ (see Eq. (2.32)), the calculations which we will do further are characterized by the order of $1/(mN_c)$. We take the chiral limit and the large N_c limit with $1/(mN_c)$ fixed and therefore the terms with multiples of $1/(mN_c)$ are in the same order.

After these preparations, we would like to come back to the averaged fermion determinant, $\overline{\mathrm{Det}}_{N_\pm}$, in Eq. (2.29). In the thermodynamic limit, $N_\pm \to \infty$, $V \to \infty$, with $N_\pm/V$ fixed, we use the formula

$$(ab)^N = \int \frac{d\lambda}{2\pi} \exp\left\{ N \log \frac{aN}{\lambda} - N + \lambda \right\} \quad , \tag{2.36}$$

which is valid for large N. Hence, we can write Eq. (2.29) as

$$\begin{aligned} \overline{\mathrm{Det}}_{N_\pm} &= \int \mathcal{D}\bar{\psi}\mathcal{D}\psi \exp \int d^4x \left\{ -\sum_f^{N_f} \bar{\psi}_f (-i\partial\!\!\!/) \psi_f \right\} \\ &\quad \times \int \frac{\lambda_+}{2\pi} \frac{\lambda_-}{2\pi} \exp\left\{ N_+ \log\left(\frac{N_+}{\lambda_+ V} \right) - N_+ \right. \\ &\quad \left. + \lambda_+ \int d^4z d\rho f(\rho) \det\Big[J_+(z,\rho) + 1 \Big] + (+ \to -) \right\} \quad . \end{aligned} \tag{2.37}$$

We note here that the saddle point in $\lambda_\pm$ in the thermodynamic limit leads to the original expression for $\overline{\mathrm{Det}}_{N_\pm}$ in Eq. (2.29).

2.4 Instanton size distribution

The instanton size distribution denoted by $f(\rho)$ originates from inter-instanton interaction. Although its exact form is still unknown, at small sizes, it is subject to the condition which the distribution function follows $f(\rho) \sim \rho^{b-5}$ [48] with b the first coefficient of the Gel-Mann–Low function, $b = \frac{11}{3} N_c - \frac{2}{3} N_f$. On the other hand, recently, several authors have proposed the shape falling off as the power of the tail $f(\rho) \sim \rho^{-n}$ at large sizes [38–40, 50]. So we adopt the special formula proposed in Ref. [36],

$$f(\rho) = f_n^{(N_f)}(\rho) = \frac{\bar{\rho}^{-1}}{\left(\frac{\rho}{\rho_1}\right)^n + \left(\frac{\rho}{\rho_2}\right)^{-b+5}} \quad . \tag{2.38}$$

This function interpolates smoothly the instanton size behaviors between the ultraviolet and infrared region. The parameters ρ_1 and ρ_2, which characterize the infrared and ultraviolet size behavior, respectively, are determined by the following conditions,

$$\int_0^\infty d\rho f(\rho) = 1 \quad , \quad \int_0^\infty d\rho f(\rho) \rho = \bar{\rho} \quad . \tag{2.39}$$

As a special case, when we take the limit $N_c \to \infty$ and $n \to \infty$, the size distribution, Eq. (2.38), become

$$f(\rho) = \delta(\rho - \bar{\rho}) \quad . \tag{2.40}$$

It means that the sizes of all instantons are fixed to the constant average size $\bar{\rho}$.

Authors in Ref [38–40, 50] have discussed the value of n. The first lattice measurements of the instanton size distribution was performed by Michael and Spencer [41] who used a cooling technique. Shuryak compered it with his measurement and concluded that the resulting distribution falls $\sim \rho^{-(d+1)}$ at large size, where $d = 4$ is just the space-time dimension [40]. He also suggested that the repulsive interaction between instantons strongly suppress large-size instantons. On the other hand, Diakonov and Petrov argued that confinement effects is kept by $\sim \rho^{-3}$ at large ρ from their analytic derivation of the instanton-induced heavy quark potential. They argue that the cooling procedure might kill confinement because the cooling annihilates closely happened instantons and anti-instantons. As a result, the cooling procedure might suppress large-size instantons stronger than their estimate.

Finally, these discussions indicate that the QCD vacuum prefer absence of large instantons to the cut-off at the Higgs mass scale formerly discussed by 't Hooft [48]. We will take several values of n for our study.

2.5 Dynamical chiral symmetry breaking

Saddle point approach

In order to calculate the averaged fermion determinant in Eq. (2.37), we have to perform integration over the fermion fields. This integral can be done for the case of one flavor, $N_f = 1$,

$$\overline{\mathrm{Det}}_{N_\pm} = \int \frac{d\lambda_+}{2\pi} \frac{d\lambda_-}{2\pi} e^{\mathcal{W}(\lambda_+, \lambda_-)} \tag{2.41}$$

where

$$\mathcal{W}(\lambda_+,\lambda_-) = \left\{ N_+ \log\left(\frac{N_+}{\lambda_+ V}\right) - N_+ + (+\to -) \right\} + \mathrm{Tr}\log\left(\frac{\not{k} + \int d\rho f_n^{(1)}(\rho) \frac{(\lambda_+ + \lambda_-) - (\lambda_+ - \lambda_-)\gamma^5}{2} \frac{4\pi^2\bar{\rho}^2}{mN_c} \left(\frac{\rho}{\bar{\rho}}\right)^2 F^2(|k|\rho)}{\not{k}} \right) \quad (2.42)$$

The saddle point of $\mathcal{W}(\lambda_+,\lambda_-)$ in the variables $\lambda_\pm$ is given by the variation,

$$\frac{\partial}{\partial\lambda_\pm}\mathcal{W}(\lambda_+,\lambda_-) = 0 \quad . \quad (2.43)$$

In order to write down Eq. (2.43) explicitly, we would like to redefine the variables $\lambda_\pm$ as

$$\lambda_\pm := \frac{mN_c}{4\pi^2\bar{\rho}^2}\mu_\pm \quad . \quad (2.44)$$

With the help of this, we obtain the condition to fix the saddle point values of $\lambda_\pm$ (corresponding to $\mu_\pm$),

$$\frac{V}{2N_\pm}\left\{ 4N_c \int \frac{d^4k}{(2\pi)^4} \frac{M_+(k^2)M_+(k^2)}{k^2 - M_+(k^2)M_-(k^2)} + \frac{mN_c}{2\pi^2\bar{\rho}^2}\mu_\pm \right\} = 1 \quad , \quad (2.45)$$

where we have defined

$$M_\pm(k^2) = \mu_\pm \int d\rho f_n^{(1)}(\rho) \left(\frac{\rho}{\bar{\rho}}\right)^2 F^2(|k|\rho) \quad . \quad (2.46)$$

We note that the mass function $M_\pm(k^2)$ has a singularity at $k^2 = 0$, if the size distribution $f(\rho)$ decreases as ρ^{-3} or more weakly at large ρ. Hence, we restrict ourselves in the region of $n > 3$.

In the case of $N_f = 1$, the integration over the fermion fields can be done exactly as shown in the previous section. However, for the case of multiple flavors, $N_f \geqq 2$, the instanton-fermion vertex becomes $2N_f$-fermionic interaction. To carry out the integral over the fermion fields, we introduce auxiliary boson fields to linearize the exponent of Eq. (2.37). This can be done using the formula [47]

$$\exp(\lambda \det J) = \int d\mathcal{B}\ \exp\left[-(N_f - 1)\lambda^{-\frac{1}{N_f-1}} (\det\mathcal{B})^{\frac{1}{N_f-1}} + \mathrm{tr}(\mathcal{B}J) \right] \quad , \quad (2.47)$$

which holds in the saddle point approximation. Here, $\mathcal{B}$ is a Hermitian $N_f \times N_f$ matrix variable, which contains scalar and pseudoscalar bosons with flavor singlet and multiplet (triplet for $N_f = 2$, and octet for $N_f = 3$), and so on. Using Eq, (2.47), we rewrite Eq. (2.37) as

$$\begin{aligned}
\overline{\mathrm{Det}}_{N_\pm} &= \int \mathcal{D}\bar{\psi}\mathcal{D}\psi \exp \int d^4x \left\{ -\sum_f^{N_f} \bar{\psi}_f(-i\partial\!\!\!/)\psi_f \right\} \\
&\quad \times \int \frac{\lambda_+}{2\pi}\frac{\lambda_-}{2\pi} \exp\left\{ N_+ \log\left(\frac{N_+}{\lambda_+ V}\right) - N_+ + (+ \to -) \right\} \\
&\quad \times \int \mathcal{B}_+\mathcal{B}_- \exp \int d^4x \int d\rho \Big\{ -(N_f-1)\left(\lambda_+ f_n^{(N_f)}(\rho)\right)^{\frac{1}{N_f-1}} (\det \mathcal{B}_+(x,\rho))^{\frac{1}{N_f-1}} \\
&\qquad + \mathrm{tr}\left(\mathcal{B}_+(x,\rho)\Big[J_+(x,\rho)+1\Big]\right) + (+ \to -) \Big\} \quad . \qquad (2.48)
\end{aligned}$$

The saddle point condition of $\lambda_\pm$ are given as

$$\lambda_\pm^{\frac{1}{N_f-1}} = \frac{1}{N_\pm} \int d^4x \int d\rho \Big(f_n^{(N_f)}(\rho) \Big)^{-\frac{1}{N_f-1}} \Big(\det \mathcal{B}_\pm(x,\rho) \Big)^{\frac{1}{N_f-1}} \quad . \qquad (2.49)$$

These conditions lead to

$$\begin{aligned}
&\overline{\mathrm{Det}}_{N_\pm} \\
&= \int \mathcal{D}\bar{\psi}\mathcal{D}\psi \exp \int d^4x \left\{ -\sum_f^{N_f} \bar{\psi}_f(-i\partial\!\!\!/)\psi_f \right\} \\
&\quad \times \int \mathcal{D}\mathcal{B}_+\mathcal{D}\mathcal{B}_- \exp \int d^4x \int d\rho \left\{ \mathrm{tr}\Big(\mathcal{B}_+(x,\rho)[J_+(x,\rho)+1]\Big) + \Big(+ \to -\Big) \right\} \qquad (2.50) \\
&\quad \times \left\{ -N_+(N_f-1)\log\left(\int d^4x \int d\rho \left(f_n^{(N_f)}(\rho) \right)^{-\frac{1}{N_f-1}} \left(\det \mathcal{B}_+(x,\rho) \right)^{\frac{1}{N_f-1}} \right) + \Big(+ \to -\Big) \right\} \quad .
\end{aligned}$$

We assume that the diagonal elements of $\mathcal{B}_\pm$ are dominant and x independent, and factorize the instanton size dependence of $\mathcal{B}_\pm$ as

$$\mathcal{B}_\pm(\rho) = f_n^{(N_f)}(\rho) \begin{pmatrix} B_{\pm,1}(\rho) & & \mathbf{0} \\ & \ddots & \\ \mathbf{0} & & B_{\pm,N_f}(\rho) \end{pmatrix} \quad . \qquad (2.51)$$

We search for a minimum point of the exponent of Eq. (2.48),

$$\frac{\partial}{\partial B_{\pm,f}(\rho)} \mathcal{W}(B_{+,f}(\rho), B_{-,f}(\rho)) = 0 \quad , \qquad (2.52)$$

where

$$
\begin{aligned}
&-\mathcal{W}(B_{+,f}(\rho), B_{-,f}(\rho)) \\
&= V\sum_f \int d\rho f_n^{(N_f)}(\rho) B_{+,f}(\rho) \\
&\quad -N_+(N_f-1)\log\left\{\int d\rho f_n^{(N_f)}(\rho)\left(\prod_f B_{+,f}(\rho)\right)^{\frac{1}{N_f-1}}\right\} + \left(+\to -\right) \\
&\quad +\sum_f \mathrm{Tr}\log\left(\frac{\not{k} + \int d\rho f_n^{(N_f)}(\rho)\frac{(B_{+,f}(\rho)+B_{-,f}(\rho))-(B_{+,f}(\rho)-B_{-,f}(\rho))\gamma^5}{2}\frac{4\pi^2\bar{\rho}^2}{mN_c}\left(\frac{\rho}{\bar{\rho}}\right)^2 F^2(|k|\rho)}{\not{k}}\right)
\end{aligned}
\tag{2.53}
$$

We shall write the condition Eq. (2.52) explicitly below. In order to do this, we would like to redefine the variables $\lambda_\pm$ by $\mu_\pm^{(N_f)}$ and $B_{\pm,f}$ by $b_{\pm,f}$ as

$$
\lambda_\pm := \left(\frac{V}{N_\pm}\right)^{N_f-1}\left(\frac{mN_c}{4\pi^2\bar{\rho}^2}\mu_\pm^{(N_f)}\right)^{N_f} \quad , \quad B_{\pm,f}(\rho) := \frac{mN_c}{4\pi^2\bar{\rho}^2} b_{\pm,f}(\rho) \quad . \tag{2.54}
$$

Introducing $M_{\pm,f}^{(N_f)}$ for convenience,

$$
M_{\pm,f}^{(N_f)}(k^2) := \int d\rho f_n^{(N_f)}(\rho) b_{\pm,f}(\rho)\left(\frac{\rho}{\bar{\rho}}\right)^2 F^2(|k|\rho) \quad , \tag{2.55}
$$

we can write the equation corresponding to Eq. (2.52) as

$$
\frac{V}{2N_\pm}\left\{4N_c\int\frac{d^4k}{(2\pi)^4}\frac{M_{+,f}^{(N_f)}(k^2)M_{-,f}^{(N_f)}(k^2)}{k^2+M_{+,f}^{(N_f)}(k^2)M_{-,f}^{(N_f)}(k^2)} + \frac{mN_c}{2\pi^2\bar{\rho}^2}\int d\rho f_n^{(N_f)}(\rho)_{\pm,f}(\rho)\right\} = 1 \quad . \tag{2.56}
$$

On the other hand, Eq. (2.49) is rewritten as

$$
\mu_\pm^{(N_f)} = \left\{\int d\rho f_n^{(N_f)}(\rho)\left(\prod_f b_{\pm,f}(\rho)\right)^{\frac{1}{N_f-1}}\right\}^{\frac{N_f-1}{N_f}} \quad . \tag{2.57}
$$

In the case of $N_f = 1$ the dynamical quark mass is given by Eq. (2.46) which corresponds to the general mass function, Eq. (2.55), with $b_{\pm,f}(\rho) = \mu_\pm f_n^{(1)}(\rho)/f_n^{(N_f)}(\rho)$. As found in Eq. (2.56) clearly, $b_{\pm,f}(\rho)$ given by $\mu_\pm f_n^{(1)}(\rho)/f_n^{(N_f)}(\rho)$ is a solution of Eq. (2.56). In the large ρ region the ratio $f_n^{(1)}(\rho)/f_n^{(N_f)}(\rho)$ goes to 1 as ρ is increased and in the small ρ region

$f_n^{(1)}(\rho)/f_n^{(N_f)}(\rho) \sim \rho^{\frac{2}{3}(N_f-1)}$. Finally we obtain the saddle point condition for general N_f expressed as

$$\mu_\pm^{(N_f)} = \mu_\pm \left\{ \int d\rho f_n^{(N_f)}(\rho) \left(\frac{f_n^{(1)}(\rho)}{f_n^{(N_f)}(\rho)} \right)^{\frac{N_f}{N_f-1}} \right\}^{\frac{N_f-1}{N_f}} \quad . \tag{2.58}$$

The mass function is given by

$$M_{\pm,f}^{(N_f)}(k^2) = M_\pm(k^2) = \mu_\pm \int d\rho f_n^{(1)}(\rho) \left(\frac{\rho}{\bar{\rho}} \right)^2 F^2(|k|\rho) \quad . \tag{2.59}$$

The mass function is given by the same function as in the one flavor case.

Schwinger-Dyson Approach to the dynamical quark mass

In the previous subsection, we have considered the saddle point of the effective action using the bosonization formalism. In that formalism we have employed the approximation where the boson field is constrained on the diagonal elements in the flavor space, Eq. (2.51). Using the obtained saddle point values we calculate physical quantities. In order to calculate physical quantities as the quark condensate $\langle\bar{\psi}\psi\rangle$, we should know the quark propagator. The quark propagator is given by

$$S_f(q) = \int d^4x d^4y \langle 0|\psi_f(x)\bar{\psi}_f(y)|0\rangle e^{-iq\cdot(x-y)} \quad . \tag{2.60}$$

We employ the Schwinger-Dyson approach to the dynamical quark mass,

$$S_f(q) = S_{0,f}(q) + S_{0,f}(q)K_f(q)S_f(q) \quad , \tag{2.61}$$

where K corresponds to the kernel contributed by one instanton and anti-instanton in the leading of $1/N_c$. As usual, Eq. (2.61) is rewritten as

$$S_f^{-1}(q) = S_{0,f}^{-1}(q) - K_f(q) \quad . \tag{2.62}$$

We write down explicitly the Schwinger-Dyson kernel as

$$K_{\pm,f}(q) = -\frac{1 \mp \gamma^5}{2} \mu_\pm^{(N_f)} \int d\rho f_n^{(N_f)}(\rho) \left(\frac{\rho}{\bar{\rho}} \right)^2 F^2(|q|\rho)$$

$$\times \prod_{g\neq f} \mu_{\pm}^{(N_f)} \frac{V}{2N_{\pm}} \left\{ 2 \int \frac{d^4k_g}{(2\pi)^4} \left(\frac{\rho}{\bar{\rho}}\right)^2 F^2(|k_g|\rho) \mathrm{Tr}\left[\frac{1\mp\gamma^5}{2} S_g(k_g)\right] + \frac{mN_c}{2\pi^2\bar{\rho}^2} \right\} , \quad (2.63)$$

where $\mu_{\pm}^{(N_f)}$ are given by Eq. (2.58). We parameterize the quark propagator,

$$S_f^{-1}(q) = \not{q} + \frac{1-\gamma^5}{2} \mathcal{M}_{+,f}^{(N_f)}(q^2) + \frac{1+\gamma^5}{2} \mathcal{M}_{-,f}^{(N_f)}(q^2) \quad , \quad (2.64)$$

which is required by the Lorentz invariance.

After some manipulations we find that

$$\mathcal{M}_{\pm,f}^{(N_f)}(q^2) = \mu_{\pm}^{(N_f)} \int d\rho f_n^{(N_f)}(\rho) \left(\frac{\rho}{\bar{\rho}}\right)^2 F^2(|q|\rho) \prod_{g\neq f} \mathcal{P}_{\pm,g}(\rho) \quad , \quad (2.65)$$

where

$$\mathcal{P}_{\pm,f}(\rho) = \mu_{\pm}^{(N_f)} \frac{V}{2N_{\pm}} \left\{ 4N_c \int \frac{d^4k}{(2\pi)^4} \left(\frac{\rho}{\bar{\rho}}\right)^2 F^2(|k|\rho) \frac{\mathcal{M}_{\mp,f}^{(N_f)}(k^2)}{k^2 + \mathcal{M}_{+,f}^{(N_f)}(k^2)\mathcal{M}_{-,f}^{(N_f)}(k^2)} + \frac{mN_c}{2\pi^2\bar{\rho}^2} \right\} . \quad (2.66)$$

In order to compare $\mathcal{M}_{\mp,f}^{(N_f)}(q^2)$ to the mass functions obtained in the bosonization procedure, Eq. (2.59), we define variables $P_{\pm,f}(\rho^2)$ as

$$P_{\pm,f}(\rho) = \prod_{g\neq f} \mathcal{P}_{\pm,g}(\rho) \quad . \quad (2.67)$$

Using the variables $P_{\pm,f}(\rho)$ we rewrite Eqs. (2.65) and (2.66) as

$$\mathcal{M}_{\pm,f}^{(N_f)}(q^2) = \mu_{\pm}^{(N_f)} \int d\rho f_n^{(N_f)}(\rho) \left(\frac{\rho}{\bar{\rho}}\right)^2 F^2(|q|\rho) P_{\pm,f}(\rho) \quad , \quad (2.68)$$

and

$$\int d\rho f_n^{(N_f)}(\rho) \left(\prod_f P_{\pm,f}(\rho)\right)^{\frac{1}{N_f-1}}$$
$$= \frac{V}{2N_{\pm}} \left\{ 4N_c \int \frac{d^4k}{(2\pi)^4} \frac{\mathcal{M}_{+,f}^{(N_f)}(k^2)\mathcal{M}_{-,f}^{(N_f)}(k^2)}{k^2 + \mathcal{M}_{+,f}^{(N_f)}(k^2)\mathcal{M}_{-,f}^{(N_f)}(k^2)} + \frac{mN_c}{2\pi^2\bar{\rho}^2} \mu_{\pm}^{(N_f)} \int d\rho f_n^{(N_f)}(\rho) P_{\pm,f}(\rho) \right\} . \quad (2.69)$$

Obviously $P_{\pm,f}(\rho) = \frac{\mu_{\pm} f_n^{(1)}(\rho)}{\mu_{\pm}^{(N_f)} f_n^{(N_f)}(\rho)}$ satisfy Eq. (2.69). With this condition the mass functions, Eq. (2.68), are given by the same equations as those in the bosonization procedure.

This suggests that the approximation for the boson field, Eq. (2.51), corresponding to the Schwinger-Dyson approach to the dynamical quark mass in the large-N_c limit.

2.6 Numerical calculations

The free parameters are the packing fraction $\bar{\rho}/\bar{R}$ with $\bar{R}^4 = V/N$, and n which is a fall-off parameter of the instanton size distribution function $f(\rho)$ in the large instanton size region.

In Fig. 2.1, we show the results of mass functions with several size distributions characterized by n. All the calculations are done with $N_c = 3$ and $N_+ = N_-$ in the results with the fixed instanton size. The mass function with $n = 3$ trivially diverges at $|k| = 0$, as we mentioned in the definition of the mass function, Eq. (2.46). This situation suggests that quarks in the instanton background with $n = 3$ are always in off-shell state and, naively, confined.

In the infrared region, $|k| < 300$ MeV, the mass function depends largely on the instanton size distribution, while in the large momentum region, $|k| > 300$ MeV, the difference is not much. With the distribution function, $n = 3$ the mass function has quite a peculiar behavior because of the logarithmic divergence of the mass function, Eq. (2.59), at $k^2 = 0$.

The thin curves in Fig. 2.1 represents the case which $n \to 0$, that is, instanton sizes are fixed to $\bar{\rho}$. The mass in this case is smaller than the cases with the distribution with a finite width. Actually, the dynamical mass at $n \to \infty$ is the lower limit of those with the finite n, as shown in Fig. 2.2. Fig. 2.2 represents the dynamical mass at $|k| = 0$ with various n of the instanton size distribution. Several curves correspond to cases of the several packing fractions. Those curves are monotonically fall off and tend to the value of the mass in the case with fixed sizes. We show the values of the dynamical mass with several the packing fraction and their lower limits at $n = 5.0$ in Table 2.1.

$\bar{\rho}/\bar{R}$	0.25	0.30	0.35	0.40
$M(0)$ [MeV]	218	330	477	665
L.L. [MeV]	176	264	380	528

Table 2.1: **The dynamical mass at $|k| = 0$ with various $\bar{\rho}/\bar{R}$ at $|k| = 0$ and $n = 5.0$. L.L. is the lower limit of $M(0)$.**

We also show the dependence of dynamical quark mass at $k^2 = 0$, $M(0)$ on the packing fraction, $\bar{\rho}/\bar{R}$, in Fig. 2.3. The dashed curve is that for the case of the fixed instanton size. The subsequent solid curves are those for various instanton size distributions specified by the power n of ρ^{-n} with $n = 6, 5$ and 4 from the bottom. The dynamical mass increases rapidly as n approaches $n \sim 3$ for a fixed packing fraction. On the other hand, the dynamical mass of quark becomes large in the dense instanton vacuum, while it becomes small in the dilute case.

Using the obtained dynamical quark masses depending on the packing fraction and the size distribution function, we calculate the vacuum quark condensate and the pion decay constant. In Fig. 2.4, we show the results of the quark condensate as a function of the packing fraction. The quark condensate is given by

$$\langle \bar{\psi}\psi \rangle = -4N_c \int \frac{d^4k}{(2\pi)^4} \frac{M(k^2)}{k^2 + M^2(k^2)} \quad . \tag{2.70}$$

A reasonable value is obtained for the packing fraction of $\bar{\rho}/\bar{R} \sim 0.3$ for the case with ρ fixed to $\bar{\rho}$ as well-known [21]. The quark condensate increases slightly with the use of the size distribution. It increases monotonically with the packing fraction, $\bar{\rho}/\bar{R}$.

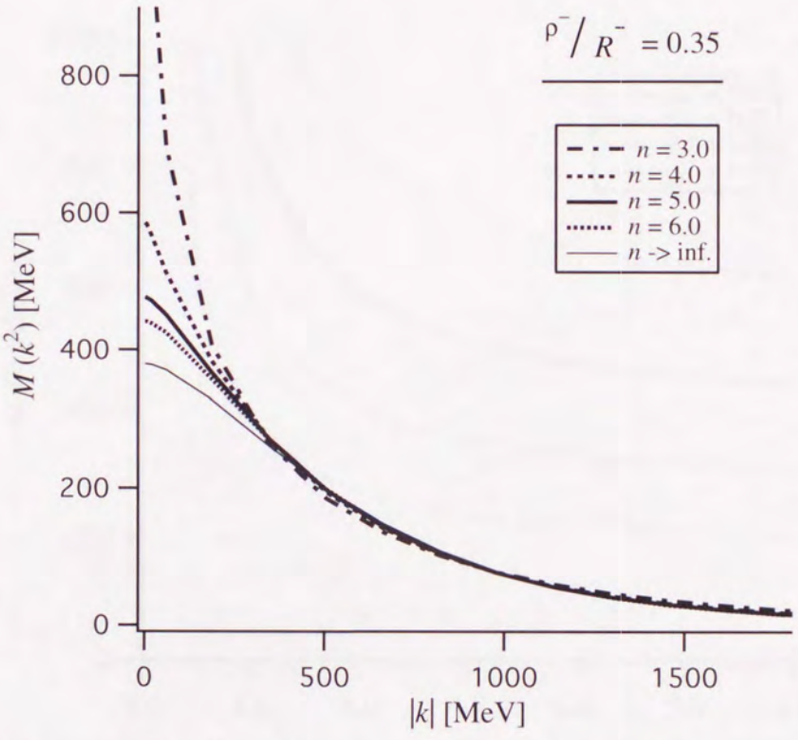

Figure 2.1: **The dynamical mass, $M(k^2)$, at the packing fraction $\bar{\rho}/\bar{R} = 0.35$.**

Curves correspond to the mass functions with $n = 3, 4, 5$ and 6 from upper side and the bottom one is an ideal case with $n \to \infty$. They are shown in unit of MeV. In $n = 3$, the mass function diverges at $|k| = 0$.

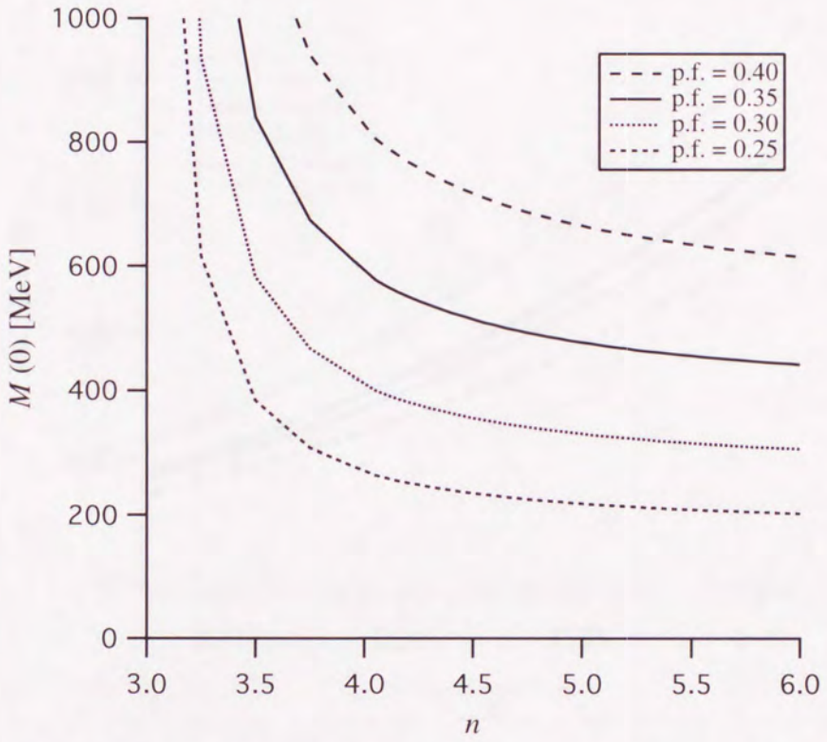

Figure 2.2: **The dynamical mass at $|k| = 0$ for the case of unfixed instanton sizes.**

n is a parameter of the instanton size distribution. In the $n < 4$ region, those curves become large rapidly, and diverge at $n = 3.0$.

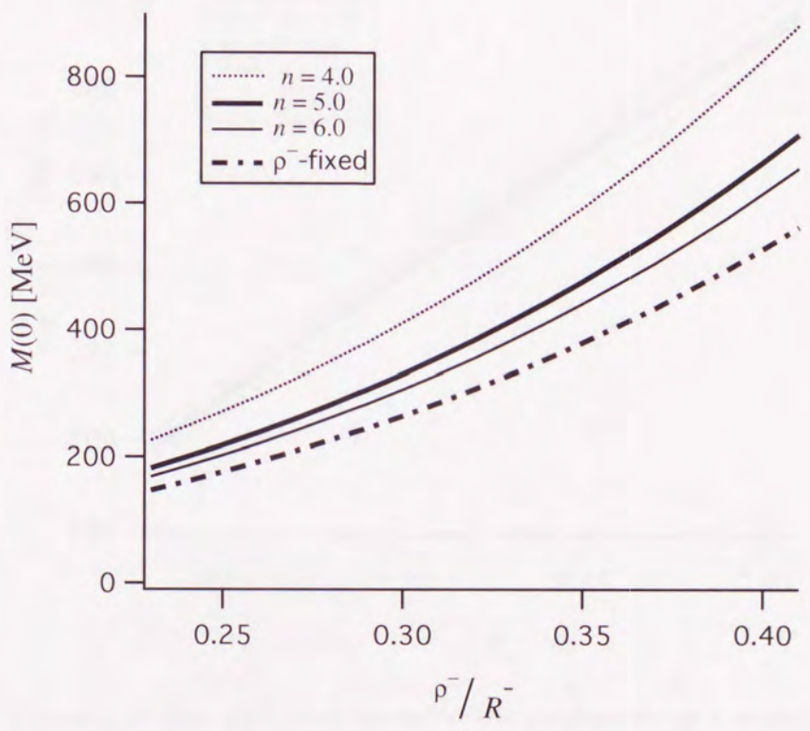

Figure 2.3: **The dynamical mass with various packing fraction $\bar{\rho}/\bar{R}$.** The dashed curve is that for the case of the fixed instanton size. The subsequent solid curves are those for various instanton size distributions specified by the power n of ρ^{-n} with $n = 6, 5$ and 4 from the bottom.

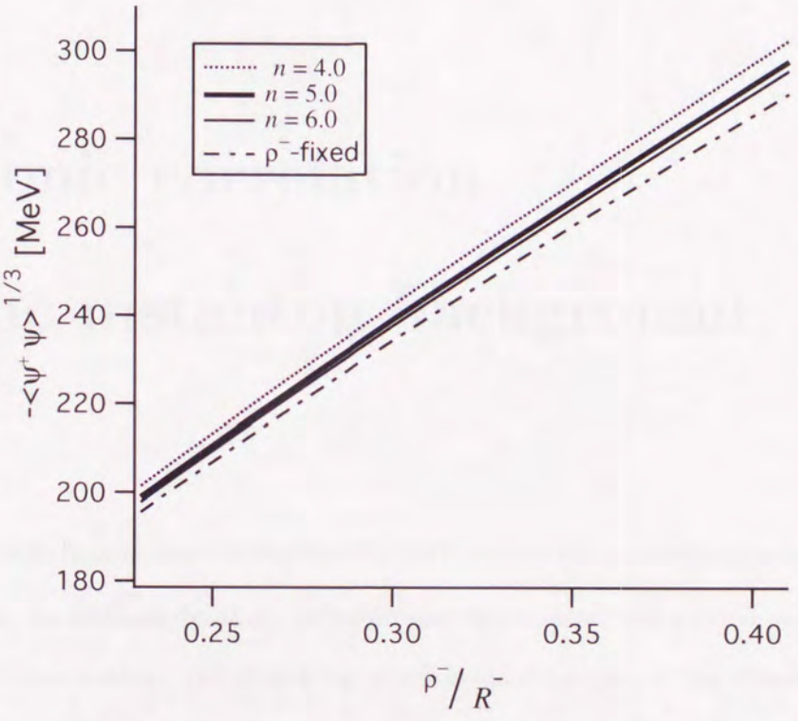

Figure 2.4: **The cubic root of the quark condensate as a function of the packing fraction.**

The dashed curve is that of the quark condensate for the case which instantons sizes are fixed to $\bar{\rho}$. The subsequent solid curves are those for various instanton size distribution specified by the power n of ρ^{-n} with $n = 6, 5$ and 4 from the bottom.

Chapter 3

Mesonic correlation in the instanton background

In a relativistic field theory, current correlation functions determine the spectrum of hadronic resonances. In addition to that, hadronic correlation functions provide a bridge between hadronic phenomenology, the underlying quark-gluon structure and the structure of the QCD vacuum. In this chapter, we will study hadronic correlations in the background of the instanton vacuum. We restrict ourselves to the case of the flavor $SU(2)_f$ and mesons as hadrons, for the testing ground of our model using the instanton ensemble with the size distribution.

To begin with, we consider the following mesonic two-point correlation functions

$$\Pi_{AB}(y-x) = \langle 0|j_A(x)j_B(y)|0\rangle \quad , \tag{3.1}$$

where $j_{A(B)}(x)$ are mesonic currents of the type

$$j_{A(B)}(x) = \delta^{ab}\bar{\psi}^a(x)\Gamma_{A(B)}\psi^b(x) \quad , \tag{3.2}$$

where a and b are color indices and Γ_A contains both isospin and Dirac matrix. Indices of gamma matrix, A and B, symbolically correspond to the mesonic channels. In order to

proceed our calculations of the mesonic correlation, Eq. (3.1), we consider the fermionic effective action coming from the result of Eq. (2.29),

$$S_{\rm eff}[\bar{\psi},\psi] = \sum_f \int d^4x \bar{\psi}(-i\partial\!\!\!/)\psi - Y_+ - Y_- \quad . \tag{3.3}$$

Here, $Y_\pm$ are the 't Hooft interaction terms in the instanton background and they are given by

$$Y_\pm = \left(\frac{V}{N_\pm}\right)^{N_f-1} \left(\frac{mN_c}{4\pi^2\bar{\rho}^2}\mu_\pm^{(N_f)}\right)^{N_f} \int d^4z\, d\rho\, f(\rho)\, \det[J_\pm(z,\rho)+1] \quad , \tag{3.4}$$

with the saddle point values, Eq. (2.54).

In the following sections, we restrict ourselves to the $SU(2)_f$ and study the pseudoscalar- and scalar-channel using the Bethe-Salpeter approach.

3.1 Quark-antiquark scattering

Considering the four-point Green function (see Appendix C), we get the Born term of the T-matrix for the quark-antiquark bound state in momentum space as,

$$T_\pm(p,k,q) = \frac{1}{2}\, \Gamma_\pm^a \otimes \Gamma_\pm^a\, \mathcal{K}_\pm(p,k,q) \quad , \tag{3.5}$$

with $\Gamma_\pm^a = \frac{1}{2}(1\mp\gamma^5)T^a$ and $T^a = (1, i\tau)$. The function $\mathcal{K}_\pm$ are the quark-antiquark scattering kernels obtained as

$$\mathcal{K}_\pm(p,k,q) = \left(\mu_\pm^{(2)}\right)^2 \frac{V}{N_\pm} \int d\rho f(\rho) \left(\frac{\rho}{\bar{\rho}}\right)^4 F(|p|\rho)F(|p+q|\rho)F(|k|\rho)F(|k+q|\rho) \quad , \tag{3.6}$$

from the calculation of the four-point Green function. Here, the momenta p, k and q are defined as shown in Fig. 3.1. We note that this kernel has a singularity at $k^2 = 0$ when the size distribution $f(\rho)$ falls off as ρ^{-5} or slower at large ρ. So we have to restrict our model discussion to $n > 5$, where n is a parameter of the instanton size distribution defined as in Eq. (2.38). Assuming that the numbers of both instantons and anti-instantons in

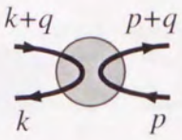

Figure 3.1: **The scattering kernel derived from the 't Hooft interaction of 4-point Green function with the instanton background.**

In this kernel, the momentum q is carried from the left hand side to the right.

the multi-instanton system are the same, $N_+ = N_-$, we sum up their contributions to the quark-antiquark T-matrix,

$$T_+(p,k,q) + T_-(p,k,q) = \sum_{I,J^P} T_{I(J^P)}(p,k,q) \quad . \tag{3.7}$$

Then we obtain the physical components of the T-matrix characterized by the quantum numbers of isospin I and spin J^P,

$$T_{I(J^P)} = P(-1)^I \, \Gamma_{I(J^P)} \otimes \Gamma_{I(J^P)} \mathcal{K}(p,k,q) \quad , \tag{3.8}$$

where we have defined the matrices $\Gamma_{I(J^P)}$ as

$$\Gamma_{I(J^P)} = (1, \tau_a, i\gamma^5, i\gamma^5\tau_a) \tag{3.9}$$

with $I(J^P) = (0(0^+), 1(0^+), 0(0^-), 1(0^-))$. Here, we have obtained $\mu := \mu_+ = \mu_-$ and $4\mathcal{K} := \mathcal{K}_+ = \mathcal{K}_-$ by considering $N_+ = N_-$. The Bethe-Salpeter equation of quark-antiquark bound state is obtained by using the scattering kernel, Eq. (3.6), as

$$T_{I(J^P)} = P(-1)^I \, \Gamma_{I(J^P)} \otimes \Gamma_{I(J^P)} \mathcal{T}_{I(J^P)}(p,k,q) \quad , \tag{3.10}$$

where

$$\mathcal{T}_{I(J^P)}(p,k,q) = \mathcal{K}(p,k,q) + \int \frac{d^4l}{(2\pi)^4} \mathcal{K}(p,l,q) \mathcal{J}_{I(J^P)}(l,q) \mathcal{T}_{I(J^P)}(l,k,q) \quad . \tag{3.11}$$

Diagrammatically, each quantity, $\mathcal{T}_{I(J^P)}$, $\mathcal{K}$ and $\mathcal{J}_{I(J^P)}$, is shown in Fig. 3.2. The quantity

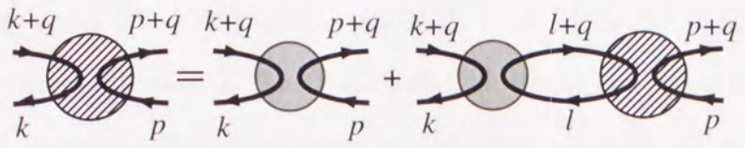

Figure 3.2: **The diagrammatic representation of the Bethe-Salpeter equation, given in Eq. (3.11).**

We define here the function $\mathcal{J}_{I(J^P)}(l,q)$ as two quark inner lines which connect the kernel $\mathcal{K}(p,l,q)$ with T-matrix $\mathcal{T}_{I(J^P)}(l,k,q)$ and carry totally momentum q.

$\mathcal{J}_{I(J^P)}$ depends on each of the mesonic quark-antiquark channels through the vertex $\Gamma_{I(J^P)}$, and connects $\mathcal{K}$ with $\mathcal{T}_{I(J^P)}$ by two dressed quark propagators given as

$$S(q) = \frac{1}{\not{q} + M(q^2)} \quad , \tag{3.12}$$

where the mass function $M(q^2)$ is given as

$$M(q^2) = \mu \int d\rho f(\rho) \left(\frac{\rho}{\bar{\rho}}\right)^2 F^2(|q|\rho) \quad . \tag{3.13}$$

The explicit form of $\mathcal{J}_{I(J^P)}$ is therefore given as

$$\mathcal{J}_{I(J^P)}(l,q) = (-1)^I \cdot 8N_c \, \frac{P\cdot(l+q)\cdot l - M((l+q)^2)M(l^2)}{\{(l+q)^2 + M((l+q)^2)\}\{l^2 + M(l^2)\}} \quad . \tag{3.14}$$

3.2 Meson propagator for fixed instanton sizes

When one fixes the instanton size to the averaged value $\bar{\rho}$, *i.e.* $f(\rho) = \delta(\rho - \bar{\rho})$, the integral of ρ in the expression of the scattering kernel $\mathcal{K}$, Eq. (3.6), can be carried out. Then we obtain the following formula

$$\mathcal{K}(p,k,q) = \mu^2 \frac{\bar{R}^4}{2} F(|p|)F(|p+q|)F(|k|)F(|k+q|) \quad , \tag{3.15}$$

with the averaged inter-instanton distance $\bar{R} := (V/N)^{-4}$. Here, the factor μ comes from redefinition of $\mu_\pm$ under $N_+ = N_-$, and is equal to $\mu_\pm^{(N_f)}$ of Eq. (2.58) when instanton sizes are fixed to the averaged value $\bar{\rho}$. The kernel, Eq. (3.15), is represented as the product of functions of each momentum. This means to add the factor $F(|p|)$ for each incoming or outgoing momentum to the vertex, schematically as in Fig. 3.3.

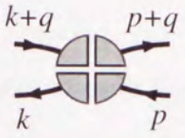

Figure 3.3: **The scattering kernel in the case when the instanton sizes are fixed to the average $\bar{\rho}$.**

We can then find the T-matrix, whose momentum dependence separates into each part, represented in the form

$$\mathcal{T}_{I(J^P)}(p,k,q) = \mu^2 \frac{\bar{R}^4}{2} F(|p|)F(|p+q|)\Big\{1 + \mathcal{S}_{I(J^P)}(q)\Big\}F(|k|)F(|k+q|) \tag{3.16}$$

(see Fig. (3.4)), where

$$\begin{aligned}\mathcal{S}_{I(J^P)}(q) \;:=\; & \mu^2 \frac{\bar{R}^4}{2}\int \frac{d^4l}{(2\pi)^4}\frac{d^4l'}{(2\pi)^4} F(|l|)F(|l+q|)F(|l'|)F(|l'+q|) \\ & \times \mathcal{J}_{I(J^P)}(l,q)\Big\{\delta^{(4)}(l-l') + \mathcal{T}(l,l',q)\mathcal{J}_{I(J^P)}(l',q)\Big\} \quad . \end{aligned} \tag{3.17}$$

The $\mathcal{S}_{I(J^P)}(q)$ plays the same role as *the meson propagator*, since it carries the meson momentum q and quantum numbers, in spite of a dimensionless quantity. Substituting Eq. (3.16) to Eq. (3.17), we find the solution of $\mathcal{S}_{I(J^P)}$,

$$\mathcal{S}_{I(J^P)}(q) = \frac{X_{I(J^P)}(q)}{1 - X_{I(J^P)}(q)} \quad , \tag{3.18}$$

$$X_{I(J^P)}(q) := \mu^2 \frac{\bar{R}^4}{2}\int \frac{d^4l}{(2\pi)^4} F^2(|l+q|)F^2(|l|)\mathcal{J}_{I(J^P)}(l,q) \quad . \tag{3.19}$$

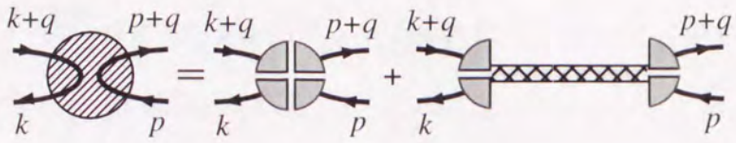

Figure 3.4: **The scattering kernel in the case when the interaction sizes are fixed to the average $\bar{\rho}$.**

To see further that the $\mathcal{S}_{I(J^P)}$ expresses mesonic propagation, let us check the Goldstone mode of it for the pseudoscalar-isotriplet channel. The explicit form of $X_{1(0^-)}$ is written as

$$X_{1(0^-)}(q) = 4N_c\bar{R}^4 \int \frac{d^4l}{(2\pi)^4} \frac{M((l+q)^2)M(l^2)\{(l+q)\cdot l + M((l+q)^2)M(l^2)\}}{\{(l+q)^2 + M^2((l+q)^2)\}\{l^2 + M^2(l^2)\}} \quad . \tag{3.20}$$

We have used here the relation $M(k^2) = \mu F^2(|k|)$. On the other hand, the ρ-fixed gap equation in the chiral limit,

$$4N_c\bar{R}^4 \int \frac{d^4l}{(2\pi)^4} \frac{M^2(l^2)}{l^2 + M^2(l^2)} = 1 \quad , \tag{3.21}$$

tells us that the $X_{1(0^-)}$ is obviously equal to one in $q^2 \to 0$. Hence, the $\mathcal{S}_{1(0^-)}$ has a singularity at zero momentum in the chiral limit.

3.3 Goldstone mode in case of unfixed instanton sizes

Return to the case that the size distribution is given in Eq. (2.38), we will show here that the pseudoscalar-isotriplet correlation function has also a singularity at zero momentum in the chiral limit, similarly as in the previous section.

We consider the mesonic correlation functions of each channel as follows,

$$\Pi_{I(J^P)}(q) = \int \frac{d^4p}{(2\pi)^4} \frac{d^4k}{(2\pi)^4} \mathcal{J}_{I(J^P)}(p,q)\mathcal{T}_{I(J^P)}(p,k,q)\mathcal{J}_{I(J^P)}(k,q) \quad . \tag{3.22}$$

When we apply the Bethe-Salpeter equation, Eq. (3.11), and the dynamical mass, $M(q^2)$, to

the integrand of the correlation function, Eq. (3.22), we get

$$\left(M(p^2) - \int \frac{d^4l}{(2\pi)^4} M(l^2) \mathcal{J}_{I(J^P)}(l,q) \mathcal{K}_{I(J^P)}(l,p,q)\right) \mathcal{J}_{I(J^P)}(p,q) \mathcal{T}_{I(J^P)}(p,k,q) \mathcal{J}_{I(J^P)}(k,q)$$
$$= M(p^2) \mathcal{J}_{I(J^P)}(p,q) \mathcal{K}(p,k,q) \mathcal{J}_{I(J^P)}(k,q) \quad . \tag{3.23}$$

On the other hand, the kernel of the Schwinger-Dyson equation, $K_f(p)$, which we considered for the quark propagator in Section 2, can be expressed by using the Bethe-Salpeter kernel $\mathcal{K}$, Eq. (3.15) as

$$K_f(p) = -\int \frac{d^4l}{(2\pi)^4} \mathrm{Tr}\left[S_{g(\neq f)}(k)\right] \mathcal{K}(l,p,0) \tag{3.24}$$

in the chiral limit (see also Appendix B). This equation is represented as in Fig. 3.5. Hence,

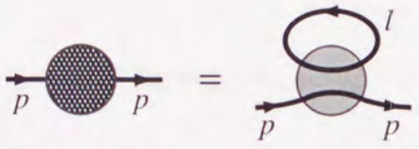

Figure 3.5: **The scattering kernel derived from the 't Hooft interaction of 4-point Green function with the instanton background.**

fig:tmatrixrfix

we can find equivalently the following mass relation in the chiral limit,

$$M(p^2) = \int \frac{d^4l}{(2\pi)^4} M(l^2) \mathcal{J}_{1(0^-)}(l,0) \mathcal{K}(l,p,0) \quad . \tag{3.25}$$

For the pseudoscalar-isotriplet channel, the bracket in the left-hand side of Eq. (3.23) vanishes at $q \to 0$ with any p. However, the right-hand side of this equation is finite. Consequently, the integrand of Eq. (3.22) , $\mathcal{J}_{1(0^-)} \mathcal{T}_{1(0^-)} \mathcal{J}_{1(0^-)}$, has to be unbounded, This means that the pseudoscalar-isotriplet correlation function, $\Pi_{1(0^-)}$, has a singularity at zero momentum in the chiral limit.

3.4 Other mesons and numerical methods

When we fixed the instanton size to the averaged value, we found that momentum dependence of the T-matrix, $\mathcal{T}_{I(J^P)}(p,k,q)$, is separable to each part. On the other hand, with the instanton size distribution, it is difficult to find such separation for the T-matrix because of the integral over instanton sizes of Eq. (3.6). When we consider $1(0^-)$ channel in the chiral limit, we avoid such a problem and we can show the Goldstone mode as in the previous two sections. However, in general, we can not perform similar calculations for other channels because of ρ-integral. Instead of extracting propagation property for each channel with the inseparable Bethe-Salpeter kernel, we compare numerically two kinds of *propagator*, that is, $\mathcal{S}_{I(J^P)}(q)$ in the separable case and

$$\mathcal{G}_{I(J^P)}(q) := \Pi_{I(J^P)}(q) N_{I(J^P)}(q) - 1 \quad , \tag{3.26}$$

in the inseparable one for each channel. Here, $N_{I(J^P)}$ is defined as

$$N_{I(J^P)}(q) := \int \frac{d^4p}{(2\pi)^4} \frac{d^4k}{(2\pi)^4} \mathcal{J}_{I(J^P)}(p,q) \mathcal{K}(p,k,q) \mathcal{J}_{I(J^P)}(k,q) \quad . \tag{3.27}$$

The function $\mathcal{G}_{I(J^P)}$ is identical to $\mathcal{S}_{I(J^P)}$ derived in the section 3.2, when the size distribution is fixed to $\bar{\rho}$.

Because of restriction from the Bethe-Salpeter kernel, Eq. (3.6), as we mentioned, we perform our numerical calculation in $n > 5$, where n is a fall-off parameter which gives dominant contribution of the form ρ^{-n} in the large instanton size region. In Figs. 3.6 and 3.7 we show the results for the function $\mathcal{S}_{1(0^+)}$ and $\mathcal{G}_{1(0^+)}$ with $n = 5.5$, which correspond to a_0 meson. The three lines are those with the packing fraction $\bar{\rho}/\bar{R}$ of 0.25, 0.35 and 0.45. The marks correspond to the data points where we numerically calculate. Similarly, we show also the result for $0(0^+)$ channel which corresponds to σ meson as in Fig. 3.8 for $\mathcal{S}_{0(0^+)}$ and in Fig. 3.9 for $\mathcal{G}_{0(0^+)}$ with $n = 5.5$, respectively. Those functions of $0(0^+)$ channel is drawn in positive region, while negative for $1(0^+)$ because of the absence of the factor $P(-1)^I$ coming

from Eq. (3.10). For various $\bar{\rho}/\bar{R}$, those lines in these figures are varied largely at small q^2. Hence, masses of those mesons may vary with $\bar{\rho}/\bar{R}$.

To extract the masses from both of $\mathcal{S}_{I(J^P)}(q)$ and $\mathcal{G}_{I(J^P)}(q)$ with the instanton size distribution, we perform the resonance fit proposed by Kugo [51]

$$\mathcal{F}_{fit}(q) = P(-1)^I \left(\frac{n^2}{q^2+m^2} + \frac{n_c^2}{q^2+m_c^2} - \frac{n_R^2}{q^2+m_R^2} \right) \quad , \tag{3.28}$$

with $m^2 \leq m_c^2 \leq m_R^2$. The factor $P(-1)^I$ is supplemented extra in our definition, since we had removed it in construction of $\mathcal{T}_{I(J^P)}(p,k,q)$ of Eq. (3.10). The first term in the right-hand side corresponds to the lowest lying meson resonance which we are interested in. The second term comes from the net effect of other resonances and the third one represents a negative background owing to the cutoff. It is difficult to see definite values of resonance masses since this fitting function has ambiguity for estimation because of many parameters. Alternatively, we use the following simplified form

$$\mathcal{F}_{fit}(q) = P(-1)^I \left(\frac{n^2}{q^2+m^2} - \frac{n_R^2}{q^2+m_R^2} \right) \quad , \tag{3.29}$$

which corresponds to the above form without the second term. We define χ^2 as

$$\chi^2 = \sum_i \left(\frac{\mathcal{S}_{I(J^P)}(q_i^2) - \mathcal{F}_{\rm fit}(q_i^2)}{\mathcal{S}_{I(J^P)}(q_i^2)} \right)^2 \quad \text{or} \quad \sum_i \left(\frac{\mathcal{G}_{I(J^P)}(q_i^2) - \mathcal{F}_{\rm fit}(q_i^2)}{\mathcal{G}_{I(J^P)}(q_i^2)} \right)^2 \quad , \tag{3.30}$$

We take eight data points in the region, $0 < q^2 < 1.7$ GeV^2, for the fit with four parameters in Eq. (3.29). In Fig. 3.10, the data points indicated by triangles correspond to $\mathcal{S}_{1(0^+)}(q)$ with the fixed instanton size and the packing fraction $\bar{\rho}/\bar{R} = 0.35$, while other data points correspond to $\mathcal{G}_{1(0^+)}(q)$ with instanton size distribution labeled by $n = 5.5 - 7.0$. As we see in Fig. 3.10, those curves are only slightly different. We obtain χ^2 for $1(0^+)$ channel, as shown in Table 3.1. We show also the results of $m_{1(0^+)}$ obtained by the fit with Eq.(3.29), as a function of the packing fraction in Fig. 3.11. The thick curve corresponds to the result with the fixed instanton size and the thin curves are obtained by the calculations with $n = 5.5, 6.0, 6.5$ and 7.0. In the region of medium and large packing fractions, The fixed

instanton size calculation gives a slightly smaller values of mass than those evaluated with the unfixed sizes. Actually, at $\bar{\rho}/\bar{R} = 0.35$, the values of mass of the fixed instanton size case is 915 MeV, while 932 MeV for the case of the size distribution with $n = 5.5$.

Two gray curves in Fig. 3.11 denote twice of the quark dynamical mass, $2M(0)$, at $|k| = 0$. The thick gray curve corresponds to the ρ fixed case, while the thin gray curve is the case with $n = 5.5$. If we regard that the dynamical mass is nearly equal to the constituent quark mass, we may say naively that the quarkonium of the $1(0^+)$ channel is the bound state of quark and antiquark in the region of the lower of those gray curves. The effect of the size distribution with finite width extends the region of the packing fraction, in which the quark and antiquark is bounded, to the smaller region of the packing fraction.

The case of $0(0^+)$ channel which corresponds to σ meson is studied also in a similar way. We show results of both $\mathcal{S}_{0(0^+)}(q)$ and $\mathcal{G}_{0(0^+)}(q)$ in Fig. 3.12, and the values of χ^2 in Table 3.2. We show also the resonance mass for various packing fractions in Fig. 3.13. At $\bar{\rho}/\bar{R} = 0.35$, the value of the resonance mass of $0(0^+)$ channel case is 442 MeV for the fixed instanton sizes, while 413 MeV for the unfixed instanton size case with $n = 5.5$. The specific point is the separation between the fixed instanton size case (thick curve) and the others (thin curves). This result represents that the lowest lying meson resonance mass does not largely depend on the fall-off parameter n. As we see in Fig.2.1, it is shown that the quark mass function in the infrared region, $|k| < 300$ MeV, is characterized by the fall-off of the large instanton size distribution, $f(\rho) \sim \rho^{-n}$. The insensitivity of the quark mass to the fall-off parameter n of the instanton size distribution suggests that the calculation of the mass of scalar quarkonium based on the Bethe-Salpeter approach is governed by the quarks in the large momentum region and, hence, the quarkonium of the scalar-isosinglet channel is a compact bound state of quark and anti-quark.

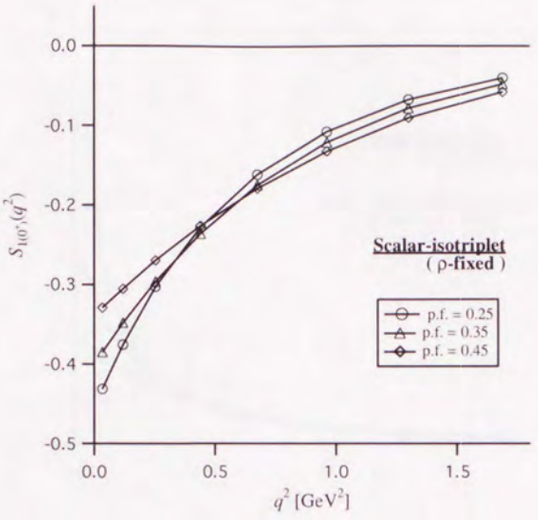

Figure 3.6: **The function $\mathcal{S}_{1(0+)}$ with various packing fractions.**

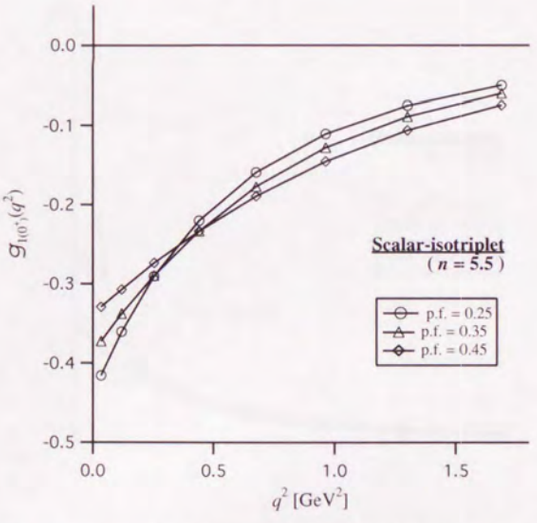

Figure 3.7: **The function $\mathcal{G}_{1(0+)}$ with various packing fractions.**

These figures represent the $1(0^+)$ channel case which corresponds to an a_0 meson. In both figures, The three lines with markers are those with the packing fraction $\bar{\rho}/\bar{R}$ of 0.25 (circle), 0.35 (triangle) and 0.45 (diamond).

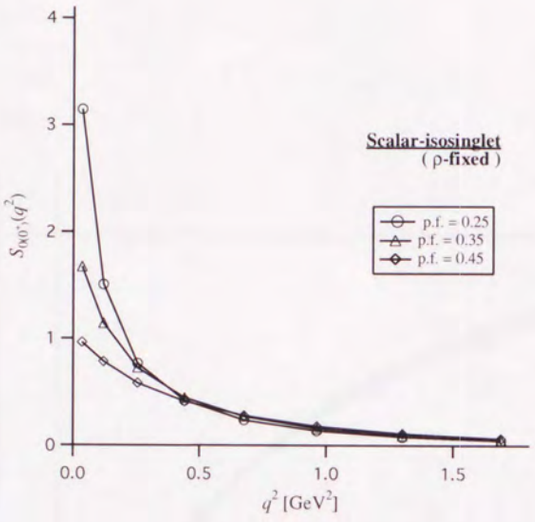

Figure 3.8: **The function $\mathcal{S}_{0(0+)}$ with various packing fractions.**

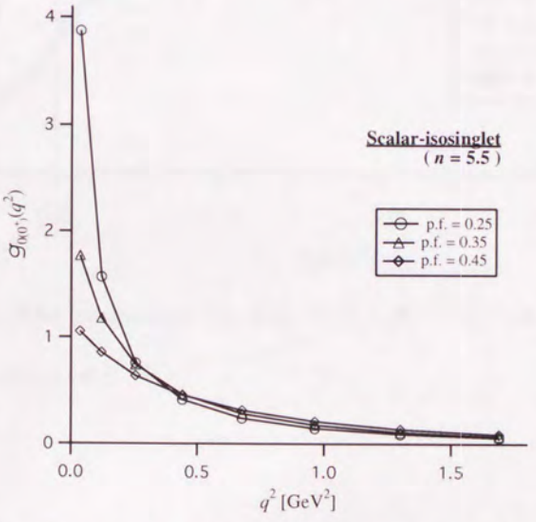

Figure 3.9: **The function $\mathcal{G}_{0(0+)}$ with various packing fractions.**

These figures represent the $0(0^+)$ channel case which corresponds to an σ meson. The three lines with markers are those with the packing fraction $\bar{\rho}/\bar{R}$ of 0.25 (circle), 0.35 (triangle) and 0.45 (diamond).

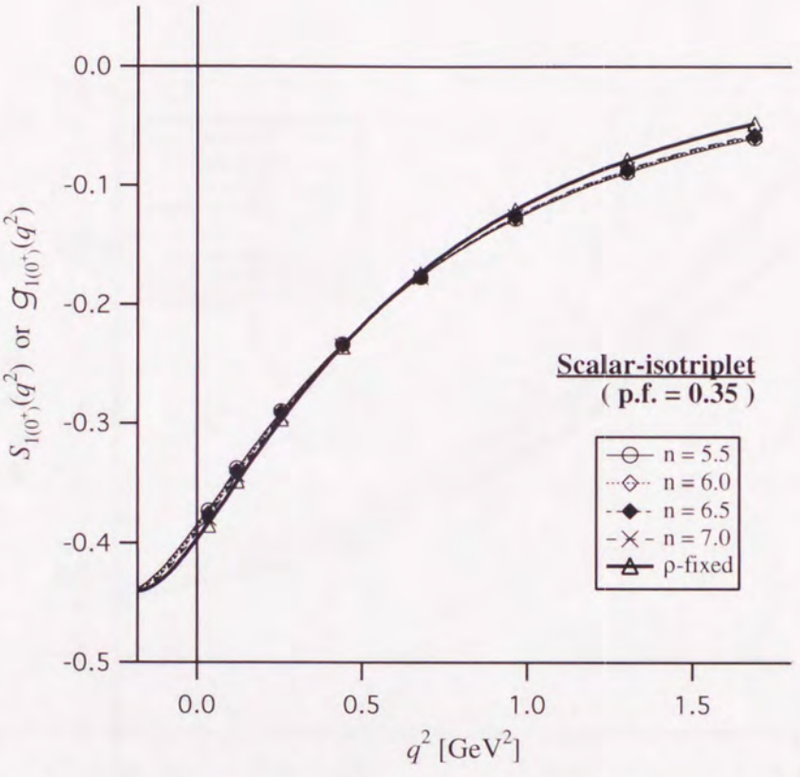

Figure 3.10: **The resonance fit, Eq.** (3.29), **for** $1(0^+)$ **channel with the packing fraction of** 0.35.

	$n = 5.5$	$n = 6.0$	$n = 6.5$	ρ-fixed
χ^2 [$\times 10^{-5}$]	6.85	7.81	8.65	14.8

Table 3.1: **The result of the resonance fit for** $1(0^+)$ **channel with the packing fraction of 0.35.**

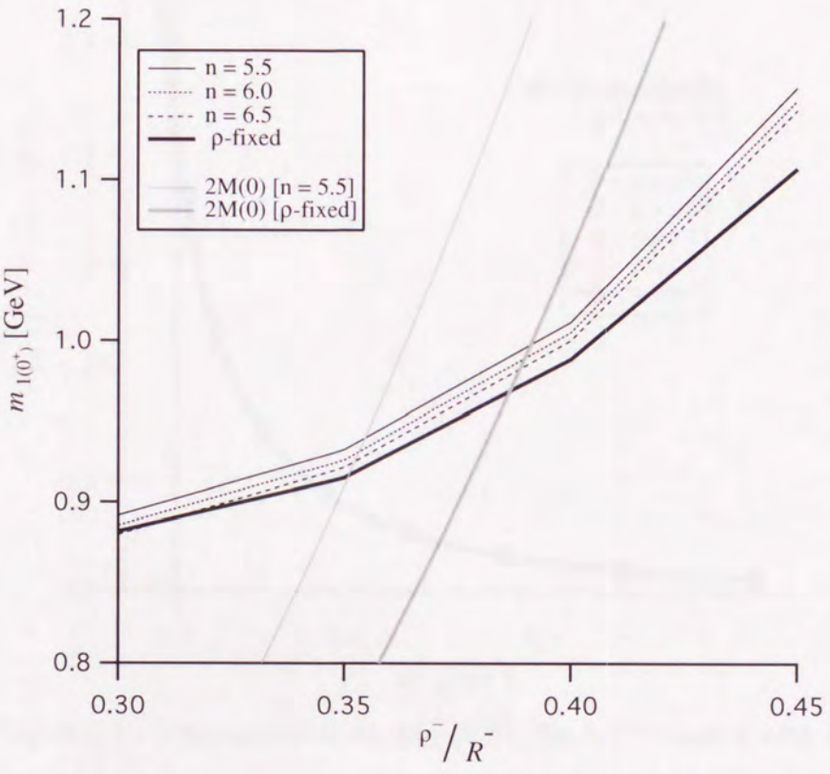

Figure 3.11: **The fitting mass for $1(0^+)$ channel with various packing fractions.**

Gray curves are twice the quark dynamical mass of zero momentum, $2M(0)$, at n = 5.5 (thin curve) and the ideal case of fixed ρ to $\bar{\rho}$ (thick curve). Each mass of the scalar-isotriplet channel characterized by n ($n = 5.5$ or $n \to \infty$) is in the bound state on the right side of each curve.

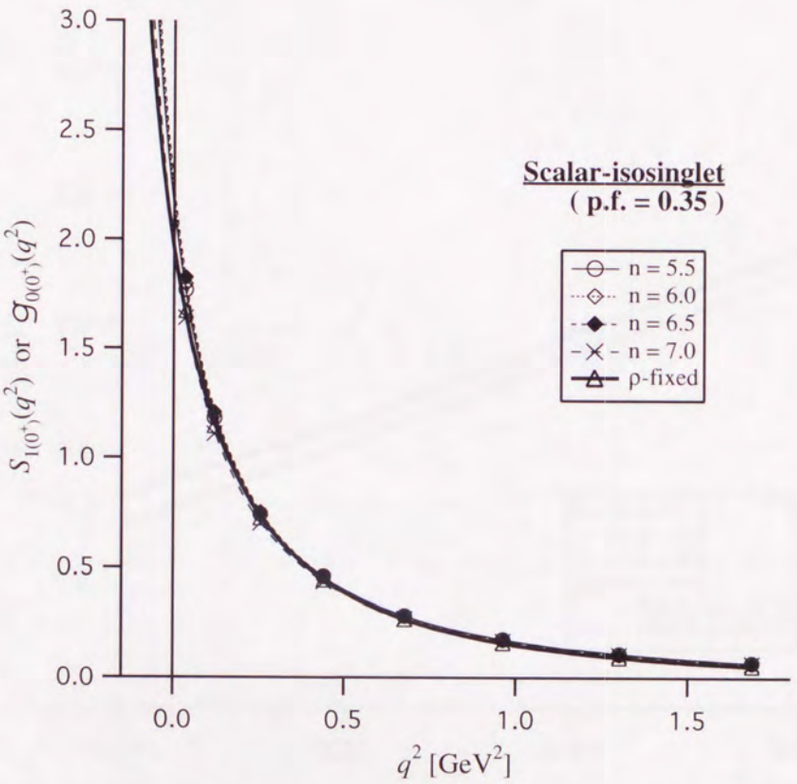

Figure 3.12: **The resonance fit, Eq.** (3.29), **for** $0(0^+)$ **channel with the packing fraction of** 0.35.

	$n = 5.5$	$n = 6.0$	$n = 6.5$	ρ-fixed
χ^2 [$\times 10^{-3}$]	1.38	1.49	1.59	11.1

Table 3.2: **The result of the resonance fit for** $0(0^+)$ **channel with the packing fraction of 0.35.**

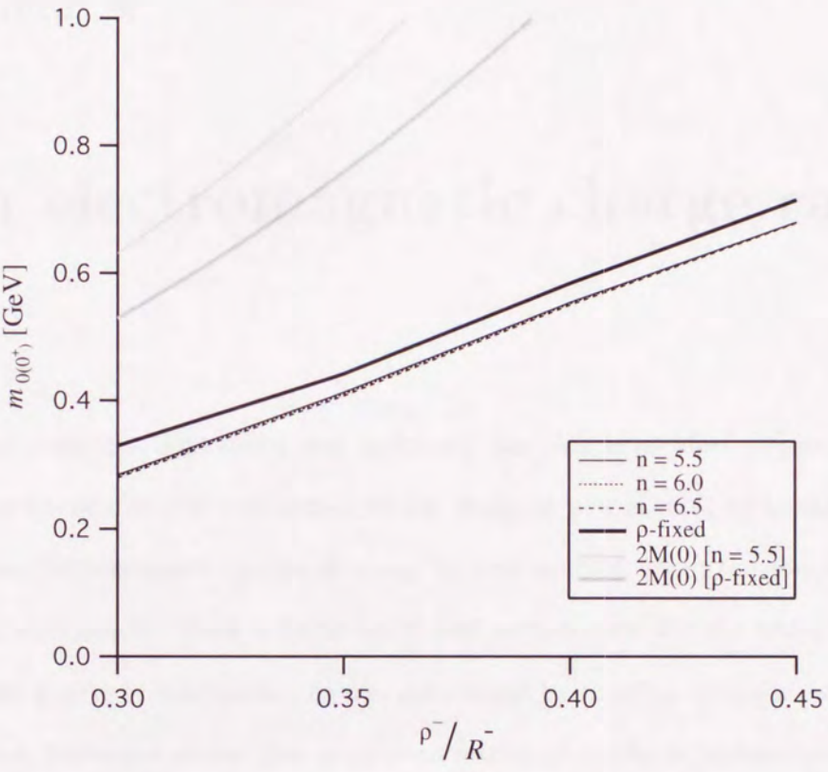

Figure 3.13: **The fitting mass for $0(0^+)$ channel with various packing fractions.**

Gray curves are twice the quark dynamical mass of zero momentum, $2M(0)$, at n = 5.5 (thin curve) and the ideal case of fixed ρ to $\bar{\rho}$ (thick curve). All of resonance masses are lower than the gray curves in the region of $0.30 < \bar{\rho}/\bar{R} < 0.45$.

Chapter 4

Pion electromagnetic charge radius

As a bound state of a light quark and antiquark, the pion is an ideal system for exploring the application of different approaches to the study of bound-state structure in QCD. In terms of the electromagnetic feature of pions, we need to think about the nontrivial coupling of photons with quarks, which is intrinsically non-perturbative. On the interaction between photons and quarks in this system, quarks are dressed by coupling with gluons dynamically. Our previous discussion means that the gluon-dressing of quarks is represented by instanton dynamics. Hence, we can not simply describe the coupling between photons and quarks but have to add the contribution from the instanton media. Such an internal structure will affect its observable properties.

When we consider the quark composite of pion, this vertex means that photons couple to quark internal lines of each flavor. It has been considered in Ref. [52] that there are several ways for coupling between them, *i.e.* 1) the one-body interaction where a photon couples to only one of quarks in the pion represented as the impulse diagram in Fig. 4.1, 2) the two-body interaction where it couples to the nontrivial current operator composed from both of two quarks shown in Fig. 4.2, and 3) a photon-quark coupling due to the vector meson

process denoted as the diagram including the modification of a photon-quark coupling, Fig. 4.3.

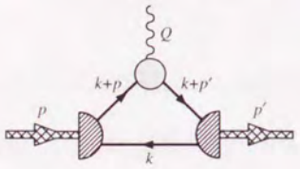

Figure 4.1: **Photon couples to one of quarks.**

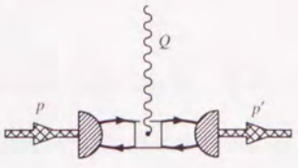

Figure 4.2: **Photon couples to two quarks simultaneously in the non-trivial way.**

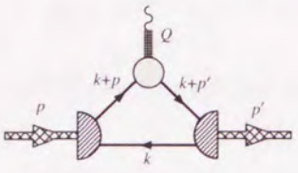

Figure 4.3: **Photon couples to a quark through the vector meson.**

We restrict ourselves to the impulse approximation where we neglect the second and the third types of the diagram. For our aim, the two-body interaction may be not relevant to our calculations. In terms of the contribution of the third diagram, it gives the contribution as the well-known vector meson dominance. So we will discuss it later in this chapter.

4.1 Bethe-Salpeter amplitude and near on mass shell

We shortly discuss the quark-pion vertex which is given as the pion Bethe-Salpeter amplitude from the formal discussion of the Bethe-Salpeter equation. However, this will be modified in accordance with our definition of the dynamical mass and the interaction kernel. We will perform such modification in the next section.

The Bethe-Salpeter equation is defined as the following form:

$$\mathcal{T}(k',k,p) = \mathcal{K}(k',k,p) + \int \frac{d^4l}{(2\pi)^4}\mathcal{K}(k',l,p)\mathcal{J}(l,p)\mathcal{T}(l,k,p) \quad . \tag{4.1}$$

We extract the Bethe-Salpeter amplitude, which is a bound-state vertex, from the T-matrix in an ordinary manner [53]. For this, we put the T-matrix in the chiral limit as

$$\mathcal{T}(k',k,p) = \frac{\Gamma_\pi(k',p)\bar{\Gamma}_\pi(k,p)}{p^2} + R(k',k,p) \quad . \tag{4.2}$$

The first term of the r.h.s is singular for p^2, while the second term is regular. So, the first term is dominant in the vicinity of the mass-shell. Then the Eq. (4.1) is reduced to

$$\Gamma_\pi(k',p)\bar{\Gamma}_\pi(k,p) = \int \frac{d^4l}{(2\pi)^4}\mathcal{K}(k',l,p)\mathcal{J}(l,p)\Gamma_\pi(l,p)\bar{\Gamma}_\pi(k,p) \quad . \tag{4.3}$$

If $\bar{\Gamma}_\pi(k,p)$ is not zero near on mass-shell, we can get the homogeneous Bethe-Salpeter equation,

$$\Gamma_\pi(k,p) = \int \frac{d^4l}{(2\pi)^4}\mathcal{K}(k,l,p)\mathcal{J}(l,p)\Gamma_\pi(l,p) \quad . \tag{4.4}$$

This equation is represented schematically in Fig. 4.4. This equation is equivalent to the gap

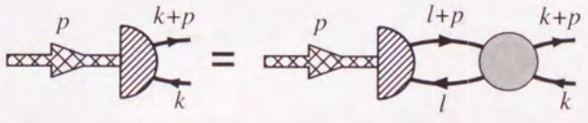

Figure 4.4: **The homogeneous Bethe-Salpeter equation.**

equation (3.25) when $p^2 = 0$. Hence, we find

$$\Gamma_\pi(k,0) \propto M(k^2) \quad , \tag{4.5}$$

Similarly, if $\Gamma_\pi(k,p) \neq 0$ for $p^2 \sim 0$, $\bar{\Gamma}_\pi(k,p)$ is subjected to the same forms of Eqs. (4.4) and (4.5).

In the diagram, we put the momenta of incoming and outgoing pion as p_μ and p'_μ. The on-mass-shell condition of pion in the chiral limit is

$$p^2 = p'^2 = 0 \quad . \tag{4.6}$$

When the photon momentum is put as $Q_\mu = p'_\mu - p_\mu$, the condition (4.6) is equivalent to the following equations

$$(p+p')^2 = -Q^2 \quad \text{and} \quad (p+p')\cdot Q = 0 \quad . \tag{4.7}$$

These relations are accepted in the Minkowski space. However, when we restrict our discussion to the Euclidean space, we have to permit an imaginary value for at least one component of momenta, except for the case where all of components are equivalently zero. We face the crucial problem which the zero-mode function $F(|p|\rho)$, which makes the dynamical mass and the interaction kernel, is not given by the imaginary value of p_μ from its definition. So we could not find any physical information from our framework.

As a cure of this difficulty, we extend it to an off shell region. We consider the vicinity of mass shell, i. e. we shift the norm of p_μ from the mass shell as $|p| = a$, with a real and small scalar constant a. The left hand side of Eqs.(4.7) is rewritten as

$$(p+p')^2 = 4a^2 - Q^2 \quad . \tag{4.8}$$

We assume then that p^2 is always equal to p'^2 for any a. This condition maintains the second relation of (4.7). From the first and second relations, both the incoming and outgoing momenta of pion are limited with

$$p^2 = p'^2 = a^2 \geq 0 \tag{4.9}$$

in contrast with Eq. (4.6).

After such modification of conditions, we reconstruct the Bethe-Salpeter amplitude of pion. The form of Eq. (4.4) is kept for any small a. Actually, when Eq. (4.2) is singular at $p^2 = a^2$,

Eq. (4.3) is rewritten as

$$\begin{aligned}
&\Gamma_\pi(k',p)\bar{\Gamma}_\pi(k,p) \\
&= \int \frac{d^4l}{(2\pi)^4}\mathcal{K}(k',l,p)\mathcal{J}(l,p)\Gamma_\pi(l,p)\bar{\Gamma}_\pi(k,p) \\
&\quad +a^2\left\{\mathcal{K}(k',k,p)+\int\frac{d^4l}{(2\pi)^4}\mathcal{K}(k',l,p)\mathcal{J}(l,p)R(l,k,p)-R(k',k,p)\right\} \quad . \qquad (4.10)
\end{aligned}$$

As a is small, the r.h.s. is equivalent to Eq. (4.4) by neglecting the terms proportional to a^2. However, the amplitude Γ_π is modified from Eq. (4.5), since p^2 is no longer zero. Expanding the pion vertex $\Gamma_\pi(k+p,k;p)$ around $p^2=0$,

$$\Gamma_\pi(k,p)=\Gamma_\pi(k,0)+\left.\frac{\partial\Gamma_\pi(k+p,k;p)}{\partial p^\mu}\right|_{p=0}p^\mu+\mathcal{O}(a^2) \quad . \qquad (4.11)$$

The first term is given as the dynamical mass from Eq. (4.5). After some manipulations, we get the Bethe-Salpeter amplitude of the following form

$$\Gamma_\pi(k,p)\propto M(k^2)+\frac{k\cdot p}{|k|}\int\frac{d^4l}{(2\pi)^4}\widetilde{\mathcal{K}}(k,l)\mathcal{J}(l,0)M(l^2)+\mathcal{O}(a^2) \quad . \qquad (4.12)$$

The function $\widetilde{\mathcal{K}}(k,l)$ in the integrand is defined as

$$\widetilde{\mathcal{K}}(k,l):=\bar{\rho}\mu_{(2)}^2\frac{\bar{R}^4}{2}\int d\rho f(\rho)\left(\frac{\rho}{\bar{\rho}}\right)^5F^2(|l|\rho)F(|k|\rho)\widetilde{F}(|k|\rho) \qquad (4.13)$$

similar to the interaction kernel $\mathcal{K}$ (Appendix E). Here, $\widetilde{F}(|k|\rho)$ is defined as the derivative of the zero-mode function,

$$\begin{aligned}
\widetilde{F}(|k|\rho) &:= \left.\frac{1}{2}\frac{dF(t)}{dt}\right|_{t=\frac{1}{2}|k|\rho} \\
&= \left[2\left(t+\frac{1}{t}\right)I_1(t)K_1(t)-2tI_0(t)K_0(t)-I_0(t)K_1(t)+I_1(t)K_0(t)\right]_{t=\frac{1}{2}|k|\rho} \qquad (4.14)
\end{aligned}$$

and it vanishes when $|k|=|l|=0$. Hence, the function $\widetilde{\mathcal{K}}(k,l)$ is regular at $|k|=|l|=0$, even when the instanton distribution parameter n is valued with any number. In the on-shell limit, $a\to 0$, Eq. (4.12) is reduced to the mass $M(k^2)$ again. In this frame work, our model is applicable to $n=5$.

4.2 Momentum symmetries of the electromagnetic vertex

Concerning the diagram Fig. 4.1, the electromagnetic vertex which gives the pion current is written as

$$\Lambda^{\mu}_{\pi^C}(p',p,Q) = 2N_c Q_{\pi^C} \int \frac{d^4k}{(2\pi)^4} \bar{\Gamma}_{\pi}(k,p') V^{\mu}(k,p',p,Q) \Gamma_{\pi}(k,p) \quad . \tag{4.15}$$

In this argument, both the traces of color and flavor matrices appeared in the triangle part of the diagram have been expanded. We have therefore written down explicitly both of the color N_c and the electromagnetic charge of the pion Q_{π^C}, respectively. The factor 2 comes from two different directions of the quark triangle loops. The V^{μ} denotes the triangle part of the impulse diagram as following form,

$$V^{\mu}(k,p',p,Q) = \mathrm{Tr}\Big[\gamma^5 S(k+p')\Gamma^{\mu} S(k+p)\gamma^5 S(k)\Big] \quad , \tag{4.16}$$

where the symbol Tr is a trace over gamma matrices. First, we simply put γ^{μ} for the quark-photon vertex Γ^{μ} for the time being. We will consider the vertex correction of Γ^{μ} later. For the nontrivial coupling between the photon and the dressed quark, we discuss in Sec. 4.3.

To extract the pion charge form factor from Eq. (4.15), we consider here several momentum symmetries of $\Lambda_{\pi^{\pm}}$, although it is in the off-shell region.

Replacing incoming pion momentum with outgoing one in Eq. (4.15) will denotes the charge conjugation. With this momentum replacement and

$$\mathcal{C}^{\dagger}\gamma^{\mu}\mathcal{C} = -\gamma^{T\mu} \quad , \tag{4.17}$$

we can find the following charge conjugation symmetry as

$$V^{\mu}(-k,-p',-p,Q) = -V^{\mu}(k,p,p',Q) \quad , \tag{4.18}$$

(See also Appendix F) and also

$$\Lambda^{\mu}_{\pi^{\pm}}(-p',-p,Q) = -\Lambda^{\mu}_{\pi^{\pm}}(p,p',Q) = \Lambda^{\mu}_{\pi^{\mp}}(p,p',Q) \quad . \tag{4.19}$$

When this is combined with a γ^5 transformation, the symmetry for the photon momentum Q is given as

$$\Lambda^{\mu}_{\pi\pm}(p', p, -Q) = -\Lambda^{\mu}_{\pi\pm}(-p, -p', -Q) = \Lambda^{\mu}_{\pi\pm}(p, p', Q) \quad . \tag{4.20}$$

The form of $\Lambda^{\mu}_{\pi C}$ which satisfies with Eqs. (4.19) and (4.20) is odd function for $(p+p')^{\mu}$ and even for Q^{μ}. So we can write the vertex as

$$\Lambda^{\mu}_{\pi\pm}(p, p', Q) \propto (p+p')^{\mu} F_{\pi} + Q^{\mu} Q \cdot (p+p') G_{\pi} \quad . \tag{4.21}$$

Both F_{π} and G_{π} are invariant functions of Q^2, $(p+p')^2$ and $(Q \cdot p + Q \cdot p')^2$.

Calculations of our model is proceeded out of the pion mass shell. However, since we mentioned in the previous section, we have put the special conditions for pion momenta. The inner product $Q \cdot (p+p')$ is, therefore, always equal to zero, similar to the on-shell case. Then, the second term of r.h.s. in Eq. (4.21) is not appear in our calculations. The final forms of the electromagnetic vertex is given as

$$\Lambda^{\mu}_{\pi\pm}(p, p', Q) \propto \pm (p+p')^{\mu} F_{\pi}(Q^2; a) \quad . \tag{4.22}$$

with a the off-shell parameter which satisfies Eq. (4.9).

We regard the function $F_{\pi}(Q^2; a)$ as the electromagnetic form factor, although it is defined in off-shell (the normalization condition is $F(0; a) = 1$). Because $F_{\pi}(Q^2; 0)$ may be a correct form factor in the on-shell limit $a \to 0$. However, the squared photon momentum, Q^2, become zero in this limit. Hence, it is justified in the vicinity of $Q^2 = 0$ in the limit of $a \to 0$.

4.3 Quark-photon vertex

We reconsider here the quark-photon interaction in the diagram. The quark-photon vertex, Γ^{μ}, satisfies the Schwinger-Dyson equation which describes both strong and electromagnetic dressing of the interaction. Solving this equation is a difficult problem that has recently begun

to be addressed [54]. In case of Nambu-Jona-Lasinio model, one can put Γ^μ into the bare vertex γ^μ, since the dynamical mass is constant. However, in our case, it is inadequate to choose the bare vertex simply. We need the vertex correction to satisfy the Ward-Takahashi identity,

$$Q_\mu \Gamma^\mu = S^{-1}(l_2) - S^{-1}(l_1) \quad , \quad Q_\mu = l_{2\,\mu} - l_{1\,\mu} \quad , \tag{4.23}$$

because of the momentum-dependent mass of quarks. We choose here the following vertex [55],

$$\Gamma^\mu(l_1, l_2) = \gamma^\mu + \frac{M(l_2^2) - M(l^2)}{l_2^2 - l_1^2}(l_1 + l_2)^\mu + \widetilde{\Gamma}^\mu(l_1, l_2) \quad , \tag{4.24}$$

and the dynamical mass $M(l^2)$ defined in Eq. (3.13). There is no term proportional to single $\not{l}_1$ or $\not{l}_2$. This vertex automatically satisfies following conditions : 1) It satisfies the Ward-Takahashi identity, 2) is free of kinematic singularity, 3) and has the same transformation as a the bare vertex, *i.e.* the charge conjugation, the Lorentz transformation and also others from symmetries included our theory.

In Eq. (4.24), the vertex, $\widetilde{\Gamma}^\mu$, is a sum of the products of momenta l_1, l_2, Q and gamma matrices, and satisfies the conditions $Q \cdot \widetilde{\Gamma} = 0$ and $\widetilde{\Gamma}^\mu(Q = 0) = 0$. So we does not need this vertex ,$\widetilde{\Gamma}^\mu$, for our context of the pion current conservation. Concerning $\widetilde{\Gamma}^\mu$, see Ref. [55, 56]

In the limit of $Q_\mu \to 0$, the Ward-Takahashi identity becomes the following form

$$\Gamma^\mu(l, l) = \frac{\partial S^{-1}(l)}{\partial\, l_\mu} \quad . \tag{4.25}$$

In case of the Ball-Chiu vertex (4.24), it reduces to

$$\Gamma^\mu(l, l) = \gamma^\mu + \frac{\partial M(l^2)}{\partial\, l_\mu} \quad . \tag{4.26}$$

The second term of the right hand side is not generally zero, except for the case where the dynamical mass $M(l^2)$ is constant for l_μ. So the vertex which satisfies the Ward-Takahashi identity contains both the bare gamma matrix and the nontrivial term which depends on

momentum. Actually, for Eq. (2.59),

$$\frac{\partial M(l^2)}{\partial\, l_\mu} = 2\bar{\rho}\mu_{(2)}\,\hat{l}^\mu \int d\rho f(\rho) \left(\frac{\rho}{\bar{\rho}}\right)^3 F(t)\widetilde{F}(t)\Big|_{t=\frac{|l|\rho}{2}} \quad , \tag{4.27}$$

where $F(t)$ and $\widetilde{F}(t)$ has been defined in Eqs. (2.34) and (4.14) and $\hat{l}^\mu$ is a unit vector of l^μ direction, does not vanish in the limit of $Q_\mu \to 0$.

4.4 The pion charge radius and numerical calculations

We found that the pion form factor in our framework is justified for small Q^2. Here, let us consider the charge radius, which is one of the important quantity to characterize pion property defined at $Q^2 = 0$ as,

$$\langle\, r_\pi^2(a)\,\rangle \;:=\; -6\,\frac{d}{dQ^2}F_\pi(Q^2;a)\Big|_{Q^2=0} \quad , \tag{4.28}$$

$$\langle\, r_\pi^2\,\rangle \;=\; \lim_{a\to 0}\langle r_\pi^2(a)\rangle \quad . \tag{4.29}$$

Our aim of calculation is to get the value of $F(Q^2;a)$ and $\langle\, r_\pi^2\,\rangle$ numerically, For this we concentrate ourselves to the Breit frame :

$$p_\mu = (0\ ,\ 0\ ,\ -Q/2\ ,\ p_4)\ ,\quad p'_\mu = (0\ ,\ 0\ ,\ +Q/2\ ,\ p_4)\ ,\quad Q_\mu = (0\ ,\ 0\ ,\ Q\ ,\ 0)\ , \tag{4.30}$$

with $Q = |Q_\mu|$. Here, the condition of momenta with off-shell parameter a, which we defined in Eq. (4.8), is represented to

$$Q^2 = 4(a^2 - p_4^2) \quad . \tag{4.31}$$

In the Breit frame, a sum of space components of p and p' vanishes so that the space component of Λ^μ is zero. Hence, our calculation is only the fourth component :

$$F(Q^2;a) = \frac{\Lambda_4(p,p',Q)}{2p_4} \quad . \tag{4.32}$$

Numerical calculations are performed at several finite values of a, since, for our accuracy, we can not calculate it when a is exactly zero.

We show the electromagnetic form factor of pions, $F_\pi(Q^2;a)$, in Fig. 4.5. Here, we have fixed the off-shell parameter a as $a^2 = 0.1$ GeV^2 and the packing fraction $\bar{\rho}/\bar{R} = 0.33$. Solid curves are those for the case of $n = 5$ and dash-dotted curves are for ρ fixed to $\bar{\rho} = 1/3$ fm. On the other hand, thin curves denote $F_\pi(Q^2;a)$ when we choose only bare vertex, γ^μ, where photons couple quark currents directly. Thick curves are those for the case of the Ball-Chiu vertex which satisfies the Ward-Takahashi identity. We add also the experimental data [57,58] denoted by dots and error bars in this figure. When $a^2 = 0.1$ GeV^2, our model calculation is applicable in the range of $0 < Q^2 < 0.4$ GeV^2 and can cover the experimental data, The curves for $n = 5$ falls off faster than those for ρ-fixed cases at the large Q^2, and the case of Ball-Chiu vertex falls more faster than the case of bare vertex. However, those curves are still drawn largely comparing with the experimental data, since a contribution of the correction term in the Bethe-Salpeter amplitude, Eq. (4.12), to the form factors is not be negligible at $a^2 = 0.1$ GeV^2. If we took $a \to 0$, such a contribution would become small. Actually, as we show in Figs. 4.6 and 4.7, the square-averaged charge radius $\langle\, r_\pi^2(a)\,\rangle$, which is determined by falling off of $F(Q^2;a)$ subjected to Eq. (4.28), get a large value when a^2 become small.

Figs. 4.6 and 4.7 represents the square-averaged charge radius $\langle\, r_\pi^2(a)\,\rangle$ with several a^2. Here, the packing fraction is fixed $\bar{\rho}/\bar{R} = 0.33$, similarly for the case in Fig. 4.5. Solid and dash-dotted lines with circles denote our result for $n = 5$ and ρ-fixed case, respectively. In both figures, $\langle\, r_\pi^2(a)\,\rangle$ looks to be converge in the small a^2 region. So, we may regard $\langle\, r_\pi^2(a)\,\rangle$ at $a^2 = 10^{-6}$ GeV^2 as $\langle\, r_\pi^2\,\rangle$ of the limiting value. We show also the values of $\langle\, r_\pi^2\,\rangle$ of our model In Table 4.1 and 4.2.

γ^μ	$n = 5$	$n = 6$	$n = 7$	ρ-fixed
$\langle\, r_\pi^2\,\rangle$ [fm^2]	0.272	0.269	0.267	0.263

Table 4.1: **Values of the pion charge radius (bare vertex)**

Ball-Chiu	$n=5$	$n=6$	$n=7$	ρ-fixed
$\langle r_\pi^2 \rangle$ [fm^2]	0.404	0.402	0.399	0.378

Table 4.2: **Values of the pion charge radius (Ball-Chiu vertex)**

Table 4.1 is for choice of γ^μ. This picture is similar to those of the Nambu−Jona-Lasinio (NJL) model without the vector meson dominance. In the NJL model, $\langle r_\pi^2 \rangle$ is given by about 0.03 fm^2 [1]. Vector mesons mediated between photons and quark currents are relevant for NJL model, since this contribution pushes up the pion charge radius to the reasonable value. However, our model calculations give $\langle r_\pi^2 \rangle$ nearly ten times larger than the NJL model, although it is still smaller than the experimental fit, $\langle r_\pi^2 \rangle_{\rm exp} = 0.439 \pm 0.008$ fm^2, in Ref. [57, 58]. This is caused by the fact that instantons strongly affect the Bethe-Salpeter amplitude which is reduced to the momentum dependent dynamical mass of a quark at $a \to 0$, while it is constant for momentum in the NJL model. Effects of the instanton size distribution seem not to be clearly appeared in this case in Fig. 4.6 or Table 4.1.

Table 4.2 shows the result for the case of the Ball-Chiu vertex which satisfies the Ward-Takahashi identity. Each result of $\langle r_\pi^2 \rangle$ is about 0.13 fm^2 larger than each of them in the case for bare vertex, and is sufficiently close to the above-mentioned experimental fit, since instantons affect it through the vertex correction. The shape of the instanton size distribution is small but appeared clearly in comparison with the former case, in the results of $\langle r_\pi^2 \rangle$.

We give also the relation between the square-averaged pion charge radius and the packing fraction of the instanton ensemble In Figs. 4.8 and 4.9. Fig. 4.8 is for the case that photons couple to quark currents forming pions directly through the bare vertex γ^μ, while Fig. 4.9 is for that with Ball-Chiu's vertex correction. Those figures tell us that the charge radius of pion shrinks in the dense instanton vacuum while it expands in the dilute case, as we found in

Fig. 2.3. The dynamical mass of quark become fat in the dense instanton vacuum. Since the Bethe-Salpeter amplitude is proportional to it at small a, the pion form factor grows in such vacuum, and hence, the charge radius become small according to Eq. (4.28). It is found that resulting values of $\langle r_\pi^2 \rangle$ in the latter case which satisfies with the Ward-Takahashi identity are good in comparison with the experimental fit around $\bar{\rho} \sim 1/3$ fm and $\bar{R} \sim 1$ fm.

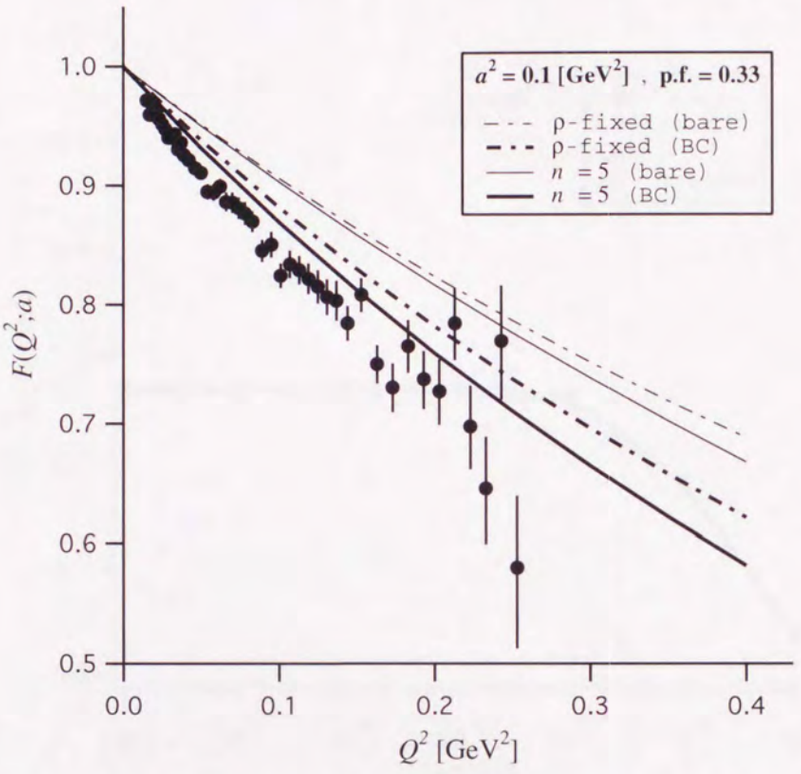

Figure 4.5: **The pion electromagnetic form factors, $F_\pi(Q^2;a)$, which depend on the off-shell parameter a.**

Solid curves are those in the case of $n = 5$, where n is the instanton size distribution parameter, and dash-dotted curves are in the case of ρ being fixed to $\bar{\rho}$. Those curves are drawn at the packing fraction $\bar{\rho}/\bar{R} = 0.33$. We add also experimental data of Ref. [57] on this figure. When $a^2 = 0.1$ GeV^2, the form factor of our model is applicable in the range $0 < Q^2 < 0.4$ GeV^2 and covers the range of the experimental data.

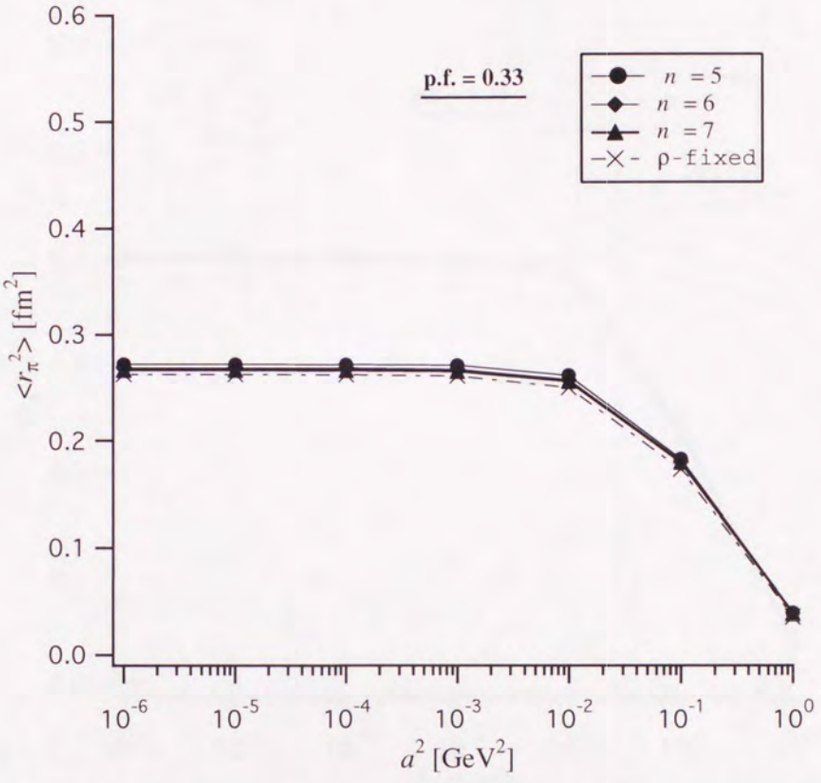

Figure 4.6: **The square average of the charge radius, $\langle r_\pi^2 \rangle$, for the bare vertex.**

This represents the case where photons couple to quark current directly. We have calculated it at the packing fraction $\bar{\rho}/\bar{R} = 0.33$. Solid lines are those of the case of $n = 5$ and dash-dotted lines are in the case of ρ being fixed to $\bar{\rho} = 1/3$ fm, respectively. Each of values of $\langle r_\pi^2(a) \rangle$ at $a^2 = 10^{-1}$ GeV^2 corresponds to each of thin curves of the previous figure 4.5.

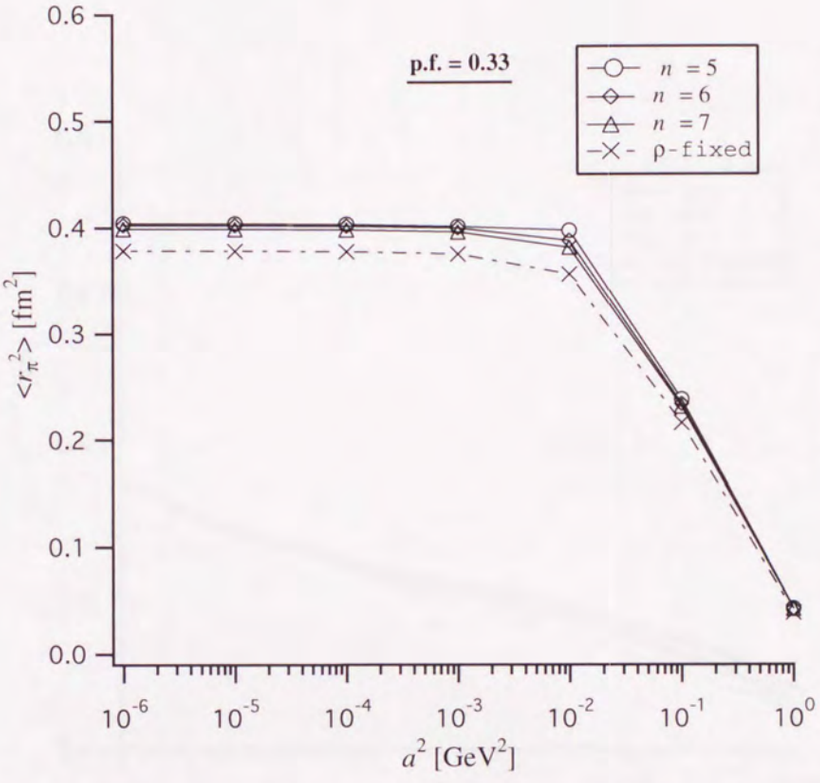

Figure 4.7: **The square average of the charge radius, $\langle r_\pi^2 \rangle$, for the Ball-Chiu vertex.**

This is the case of Ball-Chiu's vertex correction, which satisfies the Ward-Takahashi identity. Each line corresponds to the result with parameters of the instanton size distribution similar to those which was given in Fig. 4.6. We have calculated it at the packing fraction $\bar{\rho}/\bar{R} = 0.33$.

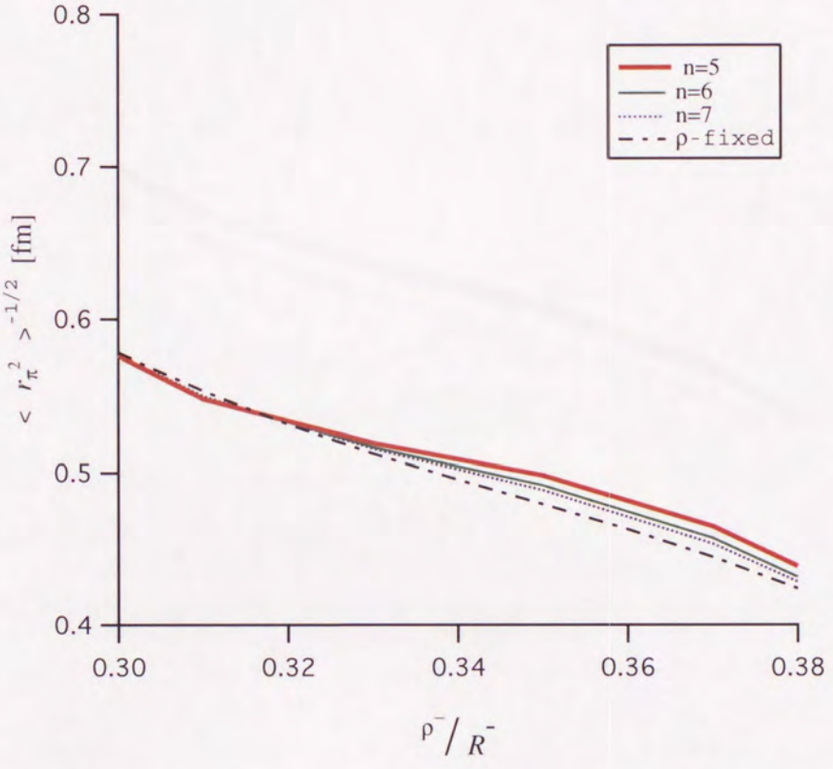

Figure 4.8: **The square average of the charge radius, $\langle r_\pi^2 \rangle$, for various values of $\bar{\rho}/\bar{R}$ with γ^μ.**

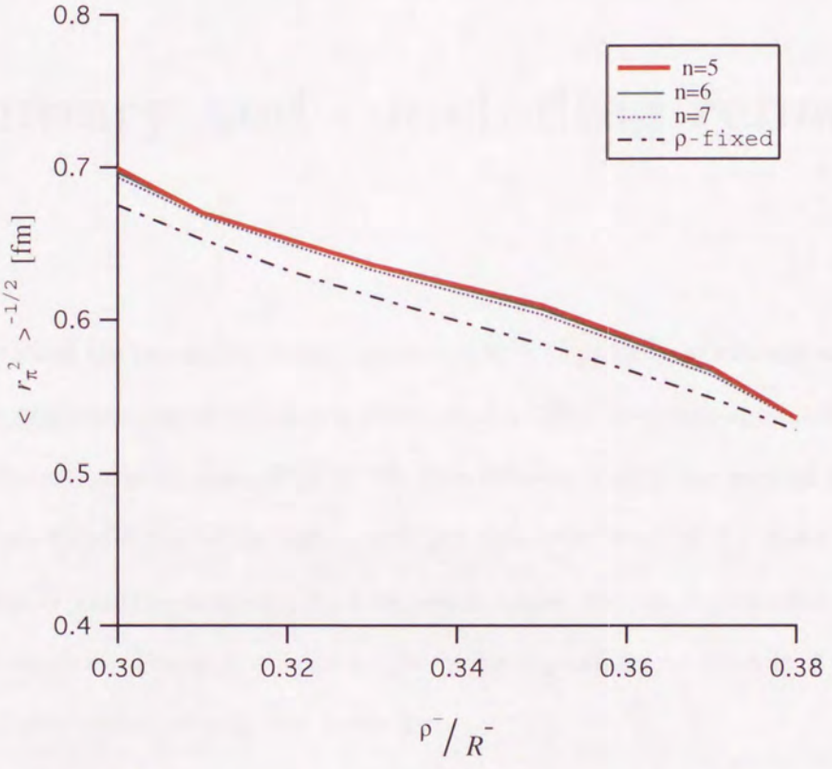

Figure 4.9: **The square average of the charge radius, $\langle r_\pi^2 \rangle$, for various values of $\bar{\rho}/\bar{R}$ with the vertex correction by Ball and Chiu.**

Chapter 5

Summary and concluding remarks

We have studied the properties of light quarks with SU(N_f) flavor symmetry and the scalar- and pseudoscalar-channel of quarkonia which are described by quark-antiquark bound state in the multi-instanton vacuum of QCD. We have followed closely the work of Diakonov and Petrov in the formulation of the light quark propagator in terms of the quark zero-mode in the presence of multi-instantons. We have newly added the size distribution of instantons into this formalism. This is motivated by the recent discussions on the role of instantons on quark confinement due to large size instantons.

In the first place, we have studied the dynamical chiral symmetry breaking of light quarks with the bosonization method. The introduction of the instanton size distribution affects the behavior of the dynamical quark mass in the infrared region. When the size distribution approaches $n = 3$ from above in the expression of $f(\rho) \propto \rho^{-n}$, the mass function is logarithmically divergent at $q^2 = 0$. This implies, in a sense, the confinement of the light quarks [59]. The difference between the dynamical quark masses calculated with various instanton size distributions is particularly large in the infrared region. We expect that the difference of the mass functions in the infrared region affects the mesonic correlation function. We have

evaluated the vacuum quark condensate, using the resulting quark propagator. A reasonable size of the chiral quantities appears with the packing fraction $\bar{\rho}/\bar{R} \sim 0.3$ for the case of the fixed instanton sizes. As the size distribution is introduced, the chiral condensate increases slightly.

We have studied the Bethe-Salpeter approach to the scalar- and pseudoscalar-mesons as bound states of quark and antiquark with SU(2) flavor in the multi-instanton vacuum in QCD. We have evaluated the mass of scalar mesons using the resonance fit of the resulting meson correlation. We have found naively that the effect of the size distribution extends the region in which the quarkonium can be the bound state of quark and antiquark to the smaller region of the packing fraction, in comparison with the case of the fixed instanton sizes. With the packing fraction $\bar{\rho}/\bar{R} = 0.35$, the scalar-isotriplet meson mass is obtained around 900 MeV. We have found also that the Bethe-Salpeter approach to the scalar-isosinglet quarkonium in the multi-instanton vacuum gives the scalar-isosinglet meson mass around 400 MeV and suggests the scalar meson is a compact bound state of quark and anti-quark.

We have studied also the electromagnetic form factor of pions and obtained the quantitative results of the pion charge radius in the instanton media with various instanton sizes. In our calculation which satisfies the Ward-Takahashi identity in the Ball-Chiu ansatz, we have obtained the square-averaged charge radius, $\langle r_\pi^2 \rangle = 0.378 - 0.404$ fm^2, around $\bar{\rho}/\bar{R} = 0.33$ and $n = 5$. It is sufficiently close to the experimental fit [57,58], although we did not introduce explicitly the contribution of the vector meson which is discussed in Nambu–Jona-Lasinio model calculations.

Appendix

A Some mathematical notations

A.1 't Hooft symbols

In terms the $SU(2)_c$ instanton solution by 't Hooft, it is convenient to use the so-called *'t Hooft symbol* which are represented as the following tensor form :

$$\eta_{a\mu\nu} = \begin{cases} \epsilon_{a\mu\nu} \\ \delta_{a\mu} \\ -\delta_{a\nu} \end{cases} \quad , \quad \bar{\eta}_{a\mu\nu} = \begin{cases} \epsilon_{a\mu\nu} & (\mu,\, \nu = 1,\, 2,\, 3) \\ -\delta_{a\mu} & (\nu = 4) \\ \delta_{a\nu} & (\mu = 4) \end{cases} \quad , \tag{A.1}$$

We define 4-vector matrices

$$\tau_\mu^\pm = (\vec{\tau}, \mp i) \quad , \tag{A.2}$$

where $\vec{\tau}$ is a vector whose components are algebra of color $SU(2)_c$, that is, the Pauli matrices, as $\vec{\tau} = (\tau_1, \tau_2, \tau_3)$. The Pauli matrices satisfy with $\tau^a \tau^b = \delta^{ab} + i\epsilon^{abc}\tau^c$, Hence, the 't Hooft symbols are appeared from multiplication of the above four-vector matrices as

$$\tau_\mu^+ \tau_\nu^- = \delta_{\mu\nu} + i\eta_{a\mu\nu}\tau^a \quad , \tag{A.3}$$

$$\tau_\mu^- \tau_\nu^+ = \delta_{\mu\nu} + i\bar{\eta}_{a\mu\nu}\tau^a \quad . \tag{A.4}$$

The 't Hooft symbols are (anti) self-dual in the vector indices

$$\eta_{a\mu\nu} = \frac{1}{2}\epsilon_{\mu\nu\alpha\beta}\eta_{a\alpha\beta} \quad , \quad \bar{\eta}_{a\mu\nu} = -\frac{1}{2}\epsilon_{\mu\nu\alpha\beta}\bar{\eta}_{a\alpha\beta} \quad , \quad \eta_{a\mu\nu} = -\eta_{a\nu\mu} \quad . \tag{A.5}$$

We have the following useful relations for contractions involving the 't Hooft symbols

$$\eta_{a\mu\nu}\eta_{b\mu\nu} = 4\delta_{ab} \quad , \tag{A.6}$$

$$\eta_{a\mu\nu}\eta_{a\mu\rho} = 3\delta_{\nu\rho} \quad , \tag{A.7}$$

$$\eta_{a\mu\nu}\eta_{a\mu\nu} = 12 \quad , \tag{A.8}$$

$$\eta_{a\mu\nu}\eta_{a\rho\lambda} = \delta_{\mu\rho}\delta_{\nu\lambda} - \delta_{\mu\lambda}\delta_{\nu\rho} + \epsilon_{\mu\nu\rho\lambda} \quad , \tag{A.9}$$

$$\eta_{a\mu\nu}\eta_{b\mu\rho} = \delta_{ab}\delta_{\nu\rho} + \epsilon_{abc}\eta_{c\nu\rho} \quad , \tag{A.10}$$

$$\eta_{a\mu\nu}\bar{\eta}_{b\mu\nu} = 0 \quad . \tag{A.11}$$

The same relations hold for $\bar{\eta}_{a\mu\nu}$, except for

$$\bar{\eta}_{a\mu\nu}\bar{\eta}_{a\rho\lambda} = \delta_{\mu\rho}\delta_{\nu\lambda} - \delta_{\mu\lambda}\delta_{\nu\rho} - \epsilon_{\mu\nu\rho\lambda} \quad . \tag{A.12}$$

Some additional relations are

$$\epsilon_{abc}\eta_{b\mu\nu}\eta_{c\rho\lambda} = \delta_{\mu\rho}\eta_{a\nu\lambda} - \delta_{\mu\lambda}\eta_{a\nu\rho} + \delta_{\nu\lambda}\eta_{a\mu\rho} - \delta_{\nu\rho}\eta_{a\mu\lambda} \quad , \tag{A.13}$$

$$\epsilon_{\lambda\mu\nu\sigma}\eta_{a\rho\sigma} = \delta_{\rho\lambda}\eta_{a\mu\nu} + \delta_{\rho\nu}\eta_{a\lambda\mu} + \delta_{\rho\mu}\eta_{a\nu\lambda} \quad . \tag{A.14}$$

A.2 Group integrations

In order to perform averages over the color $\mathrm{SU}(N_c)$ group, we need the following integrals over $U \in \mathrm{SU}(N_c)$ as

$$\int dU = 1 \quad \text{(Normalization)} \quad , \tag{A.15}$$

$$\int dU\, U_{ij}U^{\dagger}_{kl} = \frac{1}{N_c}\delta_{jk}\delta_{li} \quad , \tag{A.16}$$

$$\int dU\, U_{ij}U^{\dagger}_{kl}U_{mn}U^{\dagger}_{op} \tag{A.17}$$

$$= \frac{1}{N_c^2}\delta_{jk}\delta_{li}\delta_{no}\delta_{mp} + \frac{1}{(N_c^2-1)}\Big(\frac{1}{N_c}\delta_{jk}\delta_{li} + \delta_{kl}\delta_{ji}\Big)\Big(\frac{1}{N_c}\delta_{no}\delta_{mp} + \delta_{om}\delta_{np}\Big) \quad ,$$

Here, dU is the Haar measure, which is positive definite and left invariant on the $\mathrm{SU}(N_c)$ group. Further results are shown by Creutz [60].

In addition, it is useful to formulate them with the above mentioned four-vector matrices, Eq. (A.2),

$$\int dU\,(U\tau_\mu^{\pm}U^\dagger)_{ij} = \mp\frac{2i}{N_c}\delta_{\mu 4}\delta_{ij} \quad , \quad \int dU\,(U\tau_\mu^{\pm}\tau_\nu^{\mp}U^\dagger)_{ij} = \frac{2}{N_c}\delta_{\mu\nu}\delta_{ij} \tag{A.18}$$

$$\int dU\,(U\tau_\mu^{\pm}U^\dagger)_{ij}(U\tau_\nu^{\mp}U^\dagger)_{kl} = \frac{4}{N_c^2}\delta_{\mu 4}\delta_{\nu 4}\delta_{ij}\delta_{kl} + \frac{2}{N_c^2}\delta_{\mu\nu}\delta_{il}\delta_{kj} + \mathcal{O}\left((1/N_c)^3\right) \quad .(A.19)$$

B Schwinger-Dyson kernel with instantons

In Sect. 2, we have considered the Schwinger-Dyson equation of a quark with flavor f for discussions of the dynamical quark mass. Explicit form of the Schwinger-Dyson kernel in the instanton media is given as

$$K_{\pm,f}(q) = -\frac{1\mp\gamma^5}{2}\mu_\pm^{(N_f)}\int d\rho f_n^{(N_f)}(\rho)\left(\frac{\rho}{\bar\rho}\right)^2 F^2(|q|\rho)$$
$$\times\prod_{g\neq f}\mu_\pm^{(N_f)}\frac{V}{2N_\pm}\left\{2\int\frac{d^4k_g}{(2\pi)^4}\left(\frac{\rho}{\bar\rho}\right)^2 F^2(|k_g|\rho)\mathrm{Tr}\left[\frac{1\mp\gamma^5}{2}S_g(k_g)\right]+\frac{mN_c}{2\pi^2\bar\rho^2}\right\}, \tag{B.1}$$

with signs $\pm$ for the left- and right-handed quarks, respectively. The mass factors $\mu_\pm^{(N_f)}$ are given by Eq. (2.58).

This kernel contains (N_f-1) loops and two external lines connected in the kernel as, e. g. for $N_f \leq 3$, in Fig. (B.1). The quark in a closed loop and the one outgoing through the kernel are different flavors. In Sect. 3, we consider leading contributions of large N_c expansion for our model. Our model calculations have been restricted to $N_f \leq 2$.

When the number of instantons is equal to the number of anti-instantons, $N_+ = N_-$, we redefine the the kernel with $2K_f(q) := K_{+,f}(q) + K_{-,f}(q)$. We can then write this kernel in the chiral limit as

$$K_f(q) = -\frac{1}{4}\left(\mu^{(N_f)}\right)^{N_f}\left(\frac{2V}{N}\right)^{N_f-1}\int d\rho\, f_n^{(N_f)}(\rho)\left(\frac{\rho}{\bar\rho}\right)F^2(|q|\rho)$$
$$\times\prod_{g\neq f}\int\frac{d^4k_g}{(2\pi)^4}F^2(|k_g|\rho)\,\mathrm{Tr}[\,S_g(k_g)\,] \quad . \tag{B.2}$$

In $N_f = 2$, it is consistent with Eq. (3.24) which includes the Bethe-Salpeter kernel $\mathcal{K}$.

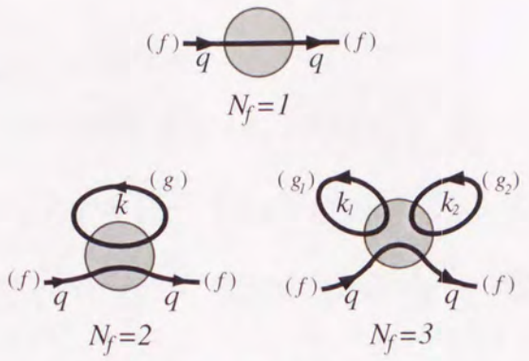

Figure B.1: **Instanton kernel with N_f flavors.**

Each kernel has (N_f-1) loops with different flavors.

C Mesonic correlations

In Section 3, to formulate the Bethe-Salpeter equation of the quark-antiquark bound state, let us consider the 4-point Green's function in momentum space as

$$G^{i_1 i_2 j_1 j_2}_{f_1 f_2 g_1 g_2}(p_1,p_2,k_1,k_2) = \langle 0|\bar{\psi}^{i_1}_{f_1}(p_1)\psi^{j_1}_{g_1}(k_1)\bar{\psi}^{i_2}_{f_2}(p_2)\psi^{j_2}_{g_2}(k_2)|0\rangle \quad , \tag{C.1}$$

where f,g are flavor indices and i,j are over gamma matrices. In the chiral limit the 't Hooft vertex, Eq. (3.4), is given as

$$\begin{aligned} Y_\pm &= \frac{N_\pm}{V}\int d^4z \int d\rho f(\rho)\det\left[\mu^{(2)}_\pm \frac{V}{N_\pm}\left(J_\pm(z,\rho)+\frac{mN_c}{2\pi^2\bar{\rho}^2}\right)\right] \\ &= \left(\mu^{(2)}_\pm\right)^2 \frac{V}{N_\pm}\int d\rho f(\rho)\int \frac{d^4k_1}{(2\pi)^4}\frac{d^4k_2}{(2\pi)^4}\frac{d^4l_1}{(2\pi)^4}\frac{d^4l_2}{(2\pi)^4} \\ &\quad \times(2\pi)^4\delta^{(4)}(k_1+k_2-l_1-l_2)\left(\frac{\rho}{\bar{\rho}}\right)^4 F(|k_1|\rho)F(|k_2|\rho)F(|l_1|\rho)F(|l_2|\rho) \\ &\quad \times\frac{1}{2!}\left\{\bar{\psi}(k_1)\frac{1\mp\gamma^5}{2}T^a\psi(l_1)\right\}\left\{\bar{\psi}(k_2)\frac{1\mp\gamma^5}{2}T^a\psi(l_2)\right\} \quad , \end{aligned} \tag{C.2}$$

where T^a is a flavor matrix which satisfies

$$T^a\otimes T^a = \frac{1}{2}(1\otimes 1-\tau^b\otimes\tau^b) \quad . \tag{C.3}$$

We get the four-point Green function with one 't Hooft vertex as follows

$$
\begin{aligned}
& G^{i_1 i_2 j_1 j_2}_{\pm, f_1 f_2 g_1 g_2}(p_1, p_2, k_1, k_2) \\
&= -(2\pi)^4 \delta^{(4)}(p_1 + p_2 - k_1 - k_2) \left(\mu^{(2)}_{\pm}\right)^2 \frac{V}{N_\pm} \\
&\quad \times \int d\rho f(\rho) \left(\frac{\rho}{\bar{\rho}}\right)^4 F(|p_1|\rho) F(|p_2|\rho) F(|k_1|\rho) F(|k_2|\rho) \\
&\quad \times S^{i_1}_{f_1}(p_1) \frac{1 \mp \gamma^5}{2} T^a S^{j_1}_{g_1}(k_1) S^{i_2}_{f_2}(p_2) \frac{1 \mp \gamma^5}{2} T^a S^{j_2}_{g_2}(k_2) \quad . \qquad \text{(C.4)}
\end{aligned}
$$

where $S^i_f(k)$ is the dressed quark propagator and its inverse operator is given as

$$
S^{-1}_f(q) = \not{q} + \left(\frac{1-\gamma^5}{2}\mu_+ + \frac{1+\gamma^5}{2}\mu_-\right) \int d\rho f(\rho) \left(\frac{\rho}{\bar{\rho}}\right)^2 F^2(|q|\rho) \qquad \text{(C.5)}
$$

from Eq. (2.64).

E Next order of off-shell Bethe-Salpeter amplitude

Expanding the quark-pion vertex $\Gamma_\pi(k+p, k; p)$ over p, we get

$$
\Gamma_\pi(k+p, k; p) = \Gamma_\pi(k, k; 0) + \left.\frac{\partial \Gamma_\pi(k+p, k; p)}{\partial p^\mu}\right|_{p=0} p^\mu + \mathcal{O}(p^2) \quad . \qquad \text{(E.1)}
$$

The first term is given as the dynamical mass from Eq. (4.5). Let us put the second term as

$$
N_\mu(k) \equiv \left.\frac{\partial \Gamma_\pi(k+p, k; p)}{\partial p^\mu}\right|_{p=0} \quad . \qquad \text{(E.2)}
$$

From Eq. (4.4), we get

$$
\begin{aligned}
N_\mu(k) &= c \int \frac{d^4 l}{(2\pi)^4} \left.\frac{\partial \mathcal{K}(k, l; p)}{\partial p^\mu}\right|_{p=0} \mathcal{J}(l; 0) M(l^2) \\
&\quad + c M(l^2) \int \frac{d^4 l}{(2\pi)^4} \mathcal{K}(k, l; 0) \left.\frac{\partial \mathcal{J}(k, l; p)}{\partial p^\mu}\right|_{p=0} + \int \frac{d^4 l}{(2\pi)^4} \mathcal{K}(k, l; 0) \mathcal{J}(l; 0) N_\mu(l) \, . \qquad \text{(E.3)}
\end{aligned}
$$

Here, $N_\mu(k)$ is a vector depending only on k_μ. So we can rewrite it as

$$
N_\mu(k) = c N(k^2) k_\mu \quad . \qquad \text{(E.4)}
$$

Then, the third term of Eq. (E.3) become zero because the integrand is odd for l_μ. Concerning the second term of Eq. (E.3),

$$\left.\frac{\partial \mathcal{J}(k,l;p)}{\partial p^\mu}\right|_{p=0} = -\frac{l_\mu + M(l^2)\widetilde{M}_\mu(l)}{\{l^2 + M^2(l^2)\}^2} \quad , \tag{E.5}$$

where

$$\widetilde{M}_\mu(l) \equiv \left.\frac{\partial M((l+p)^2)}{\partial p^\mu}\right|_{p=0} \quad . \tag{E.6}$$

Since the function $\widetilde{M}_\mu(l)$ also depends only on momentum l, we can find that the integrand of the second term of Eq. (E.3) also proportional to l_μ and therefore the integral is equal to zero. Thus, we can get

$$N(k^2)k_\mu = \int \frac{d^4l}{(2\pi)^4}\mathcal{J}(l;0)M(l^2)\left.\frac{\partial \mathcal{K}(k,l;p)}{\partial p^\mu}\right|_{p=0} \quad . \tag{E.7}$$

The definition of the kernel in the instanton background has already been obtained as

$$\mathcal{K}(k,l;p) = \mu_{(2)}^2\frac{\bar{R}^4}{2}\int d\rho f(\rho)\left(\frac{\rho}{\bar{\rho}}\right)^4 F(|k+p|\rho)F(|k|\rho)F(|l+p|\rho)F(|l|\rho) \quad . \tag{E.8}$$

Therefore,

$$\begin{aligned}&\left.\frac{\partial \mathcal{K}(k,l;p)}{\partial p^\mu}\right|_{p=0} \\ &= \mu_{(2)}^2\frac{\bar{R}^4}{2}\int d\rho f(\rho)\left(\frac{\rho}{\bar{\rho}}\right)^4 F(|k|\rho)F(|l|\rho)\left.\frac{\partial}{\partial p^\mu}F(|k+p|\rho)F(|l+p|\rho)\right|_{p=0} \quad .\end{aligned} \tag{E.9}$$

Here,

$$\begin{aligned}&\left.\frac{\partial}{\partial p^\mu}F(|k+p|\rho)F(|l+p|\rho)\right|_{p=0} \\ &= \left.\frac{\partial F(|k+p|\rho)}{\partial p^\mu}F(|l+p|\rho)\right|_{p=0} + F(|k+p|\rho)\left.\frac{\partial F(|l+p|\rho)}{\partial p^\mu}\right|_{p=0} \quad .\end{aligned} \tag{E.10}$$

The second term is proportional to l_μ and vanishes in the integration of Eq. (E.7). On the other hand,

$$\begin{aligned}\left.\frac{\partial F(|k+p|\rho)}{\partial p^\mu}\right|_{p=0} &= \left.\frac{\partial\, t}{\partial p^\mu}\cdot\frac{\partial F(|k+p|\rho)}{\partial t}\right|_{p=0} = \left.\frac{\partial\, t}{\partial p^\mu}\cdot\frac{dF(t)}{dt}\right|_{p=0} \\ &= \rho\frac{k^\mu}{|k|}\left[2\left(t+\frac{1}{t}\right)I_1(t)K_1(t) - 2tI_0(t)K_0(t) - I_0(t)K_1(t) + I_1(t)K_0(t)\right],\end{aligned} \tag{E.11}$$

where

$$\begin{aligned} t &\equiv \frac{1}{2}|k+p|\rho \quad , \\ \frac{\partial\, t}{\partial p^\mu} &= \frac{\rho}{2}\frac{\partial}{\partial p^\mu}|k+p| = \frac{\rho}{2}\,\frac{(k+p)^\mu}{|k+p|} \quad , \\ \frac{dF(t)}{dt} &= 2\left[2\left(t+\frac{1}{t}\right)I_1(t)K_1(t) - 2tI_0(t)K_0(t) - I_0(t)K_1(t) + I_1(t)K_0(t)\right] . \end{aligned} \tag{E.12}$$

Rewriting Eq. (E.12) as

$$\left.\frac{\partial F(|k+p|\rho)}{\partial p^\mu}\right|_{p=0} = \rho\widetilde{F}(|k|\rho)\frac{k^\mu}{|k|} \quad , \tag{E.13}$$

or equivalently as

$$\widetilde{F}(|k|\rho) = \frac{1}{2}\left.\frac{dF(t)}{dt}\right|_{t=\frac{1}{2}|k|\rho} \quad , \tag{E.14}$$

the derivative of the kernel, Eq. (E.9), is

$$\begin{aligned} \left.\frac{\partial\mathcal{K}(k,l;p)}{\partial p^\mu}\right|_{p=0} &= \frac{k_\mu}{|k|}\widetilde{\mathcal{K}}(k,l) \quad , \\ \widetilde{\mathcal{K}}(k,l) &\equiv \mu_{(2)}^2\frac{\bar{R}^4}{2}\int d\rho f(\rho)\left(\frac{\rho}{\bar{\rho}}\right)^4 \rho F^2(|l|\rho)F(|k|\rho)\widetilde{F}(|k|\rho) \quad . \end{aligned} \tag{E.15}$$

Hence,

$$N(k^2)k_\mu = \frac{k_\mu}{|k|}\int\frac{d^4l}{(2\pi)^4}\widetilde{\mathcal{K}}(k,l)\mathcal{J}(l;0)M(l^2) \quad . \tag{E.16}$$

Substituting Eqs. (4.5) and (E.16) with Eq. (E.1), we finally get

$$\Gamma_\pi(k+p,k;p) = cM(k^2) + c\,\frac{k\cdot p}{|k|}\int\frac{d^4l}{(2\pi)^4}\widetilde{\mathcal{K}}(k,l)\mathcal{J}(l;0)M(l^2) + \mathcal{O}(p^2) \quad . \tag{E.17}$$

F Momentum symmetry under charge conjugation and γ_5

When we consider momentum flow in the system, it is convenient to rewrite the incoming and the outgoing momenta to the center of mass and the relative momenta as

$$P_\mu := p'_\mu + p_\mu \quad , \quad Q_\mu := p'_\mu - p_\mu \quad , \tag{F.1}$$

respectively. We define new variables as

$$l_\mu := k_\mu + p_\mu = k_\mu + P_\mu - \frac{Q_\mu}{2} \quad , \quad l'_\mu := k_\mu + p'_\mu = k_\mu + P_\mu + \frac{Q_\mu}{2} \quad . \tag{F.2}$$

The momentum l_μ and l'_μ represent the quark momenta shown in the diagram, Fig. 4.1.

When we choose the Ball-Chiu vertex as $\Gamma^\mu(l,l')$, we find the following relation,

$$\begin{aligned} \mathcal{C}^\dagger\Gamma^\mu(l',l)\mathcal{C} &= \mathcal{C}^\dagger\gamma^\mu\mathcal{C} + \mathcal{C}^\dagger\frac{M(l'^2)-M(l^2)}{l'^2-l^2}(l'+l)^\mu\mathcal{C} \\ &= -\gamma^{T\mu} - \frac{M(l^2)-M(l'^2)}{l^2-l'^2}(-l-l')^\mu \\ &= -\Gamma^{T\mu}(-l,-l') \quad . \end{aligned} \tag{F.3}$$

Similarly,

$$\begin{aligned} \gamma_5^\dagger\Gamma^\mu(l',l)\gamma_5 &= \gamma_5^\dagger\gamma^\mu\gamma_5 + \gamma_5^\dagger\frac{M(l'^2)-M(l^2)}{l'^2-l^2}(l'+l)^\mu\gamma_5 \\ &= -\gamma^\mu - \frac{M(l^2)-M(l'^2)}{l^2-l'^2}(-l-l')^\mu \\ &= -\Gamma^\mu(-l,-l') \quad . \end{aligned} \tag{F.4}$$

These relations is also satisfied when we choose γ^μ as Γ^μ.

Let us consider the for the vertex V^μ, Eq. (4.16), which represent the triangle part of the impulse diagram, Fig. 4.1. The vertex V^μ is reduced to

$$\begin{aligned} & V^\mu(k,P,Q) \\ &= \mathrm{Tr}\left[\gamma^5 S(k+P+\frac{Q}{2})\Gamma^\mu(k+P+\frac{Q}{2},k+P-\frac{Q}{2})S(k+P-\frac{Q}{2})\gamma^5 S(k)\right] \\ &= \mathrm{Tr}\Big[\mathcal{C}\mathcal{C}^\dagger\gamma^5\mathcal{C}\mathcal{C}^\dagger S(k+P+\frac{Q}{2})\mathcal{C}\mathcal{C}^\dagger\mathcal{C}\mathcal{C}^\dagger\Gamma^\mu(k+P+\frac{Q}{2},k+P-\frac{Q}{2}) \\ &\qquad \times \mathcal{C}\mathcal{C}^\dagger S(k+P-\frac{Q}{2})\mathcal{C}\mathcal{C}^\dagger\mathcal{C}\mathcal{C}^\dagger\gamma^5 S(k)\mathcal{C}\mathcal{C}^\dagger\Big] \\ &= -\mathrm{Tr}\left[\gamma_5^T S^T(-k-P-\frac{Q}{2})\Gamma^{T\mu}(-k-P+\frac{Q}{2},-k-P-\frac{Q}{2})S^T(-k-P+\frac{Q}{2})\gamma_5^T S^T(-k)\right] \\ &= -\mathrm{Tr}\left[\gamma^5 S(-k-P+\frac{Q}{2})\Gamma^\mu(-k-P+\frac{Q}{2},-k-P-\frac{Q}{2})S(-k-P-\frac{Q}{2})\gamma^5 S(-k)\right] \\ &= -V^\mu(-k,-P,Q) \\ &= -\mathrm{Tr}\Big[\gamma^5\gamma^5\gamma^5 S(-k-P+\frac{Q}{2})\gamma^5\gamma^5\Gamma^\mu(-k-P+\frac{Q}{2},-k-P-\frac{Q}{2}) \\ &\qquad \times \gamma^5\gamma^5 S(-k-P-\frac{Q}{2})\gamma^5\gamma^5\gamma^5 S(-k)\gamma^5\gamma^5\Big] \\ &= \mathrm{Tr}\left[\gamma^5 S(k+P-\frac{Q}{2})\Gamma^\mu(k+P-\frac{Q}{2},k+P+\frac{Q}{2})S(k+P+\frac{Q}{2})\gamma^5 S(k)\right] \end{aligned} \tag{F.5}$$

$$= V^\mu(k, P, -Q) \quad . \tag{F.6}$$

Hence,

$$V^\mu(k, P, Q) = -V^\mu(-k, -P, Q) = V^\mu(k, P, -Q) \quad . \tag{F.7}$$

Bibliography

[1] S. Klimt, M. Lutz, U. Vogl and W. Weise, Nucl. Phys. **A516** (1990) 429.

[2] UKQCD Collaboration (G.S. Bali *et al.*), Phys. Lett. **B309** (1993) 378.

[3] J. Sexton, A. Vaccarino and D. Weingarten, Phys. Rev. Lett. **75** (1995) 4563.

[4] W. Lee and D. Weingarten, Phys. Rev. **D61** (1999) 014015.

[5] J. Weinstein and N. Isgur, Phys. Rev. Lett. **48** (1982) 65; Phys. Rev. **D27** (1983) 588; *ibid.* **D41** (1990) 2236.

[6] J.A. Oller, E. Oset and J.R. Peláez, Phys. Rev. **D59** (1999) 074001.

[7] M. Ishida, Prog. Theor. Phys. **101** (1999) 661.

[8] T. Hatsuda and T. Kunihiro, Phys. Rep. **247** (1994) 221.

[9] A. A. Belavin, A. M. Polyakov, A. A. Schwartz and Y. S. Tyupkin, Phys. Lett. **B59** (1975) 85.

[10] A. M. Polyakov, Phys. Lett. **B59** (1975) 79.

[11] R. Jackiw and C. Rebbi, Phys. Rev. Lett. **37** (1976) 172.

[12] C. G. Callan, R. Dashen and D. J. Gross, Phys. Lett. **B63** (1976) 334.

[13] A. Polyakov, Nucl. Phys. **B120** (1977) 429.

[14] G. 't Hooft, Phys. Rev. Lett. **37** (1976) 8.

[15] E. Witten, Nucl. Phys. **B149** (1979) 285.

[16] G. Veneziano, Nucl. Phys. **B159** (1979) 213.

[17] E. V. Shuryak, Nucl. Phys. **B198** (1982) 83.

[18] E. V. Shuryak, Nucl. Phys. **B214** (1983) 237.

[19] E. Ilgenfritz and M. Müller-Preussker, Nucl. Phys. **B184** (1981) 443.

[20] D. I. Diakonov and V. Yu. Petrov, Nucl. Phys. **B245** (1984) 259.

[21] D. I. Diakonov, V. Yu. Petrov, Nucl. Phys. **B272** (1986) 457.

[22] Y. Nambu, Phys. Rev. **D10** (1974) 4262.

[23] G. 't Hooft, *High Energy Physics*, ed. A. Zichichi (Editorice Compositori, Bologna, 1975).

[24] S. Mandelstam, Phys. Rep. **C23** (1976) 245.

[25] G. 't Hooft, Nucl. Phys. **B190** (1981) 455.

[26] T. Suzuki, Prog. Theor. Phys. **80** (1988) 929;

[27] T. Suzuki, Prog. Theor. Phys. **81** (1989) 752.

[28] S. Maedan and T. Suzuki, Prog. Theor. Phys. **81** (1989) 229.

[29] N. Seiberg and E. Witten, Nucl. Phys. **B426** (1994) 19.

[30] N. Seiberg and E. Witten, Nucl. Phys. **B431** (1994) 484.

[31] H. Suganuma, K. Itakura, H. Toki, O. Miyamura, Proc. of Int. Workshop on *Nonperturbative Approaches to QCD*, Trento, Italy, 10-29 Jul. (1995).

[32] F. Araki, H. Suganuma, H. Toki, Proc. of Int. Symposium on *Innovative Computational Methods in Nuclear Many-Body Systems* (INNOCOM 97),10-15 Nov., Osaka, Japan, (1997).

[33] M. Feurstein, H. Markum and S. Thurner, Phys. Lett. **B396** (1997) 203.

[34] M. N. Chernodub and F. V. Gubarev, JETP Lett. **62** (1995) 100.

[35] A. Hart and M. Teper, Phys. Lett. **B371** (1995) 261.

[36] M. Fukushima, S. Sasaki, H. Suganuma, A. Tanaka, H. Toki and D. Diakonov, Phys. Lett. **B399** (1997) 141; M. Fukushima, A. Tanaka, S. Sasaki, H. Suganuma, H. Toki and D. Diakonov, Nucl. Phys. **B53** (Proc. Suppl.) (1997) 494.

[37] M. Fukushima, H. Suganuma, H. Toki, Phys. Rev. **D60** (1999) 094504.

[38] D. I. Diakonov and V. Yu. Petrov, Proc. of International Workshop on *Nonperturbative Approaches to Quantum Chromodynamics*, Treno, Italy, Jul. 10-29, (PNPI, 1995) 239.

[39] D. I. Diakonov and V. Yu. Petrov, in *Continuous Advances in QCD 1996*, (World Scientific, 1996).

[40] E. V. Shuryak, Phys. Rev. **D52** (1995) 5370.

[41] C. Michael and P.S. Spencer, Phys. Rev. **D50** (1994) 7570; *ibid.* **D52** (1995) 4691; Nucl. Phys. **B** (Proc. Suppl.) **42** (1995) 261.

[42] M. F. Atiyah, N. J. Hitchin, V. G. Drinfeld and Y. I. Manin, Phys. Lett. **A65** (1977) 185.

[43] E. Witten, Phys. Rev. Lett. **38** (1977) 121.

[44] R. Jackiw, C. Nohl and C. Rebbi, Phys. Rev. **D15** (1977) 1642.

[45] M. Atiyah and I. Singer, Ann. Math. **87** (1968); **93** (1971) 119.

[46] A. Schwartz, Phys. Lett. **67B** (1977) 172.

[47] D. I. Diakonov, M. V. Polyakov and C. Weiss, Nucl. Phys. **B461** (1996) 539.

[48] G. 't Hooft, Phys. Rev. **D14** (1976) 3432; *ibid.* **D18** (1978) 2199.

[49] D. I. Diakonov and V. Yu. Petrov, in *Quark Cluster Dynamics*, Lecture Notes in Physics **417**, edited by K. Goeke et al, (Springer-Verlag, 1992) 288, and References therein.

[50] N. O. Agasyan and Yu. A. Simonov, Mod. Phys. Lett. **A10** (1995) 1755; N. O. Agasyan, Phys. Atom. Nucl. **59** (1996) 297.

[51] T. Kugo, *Dynamical Symmetry Breaking*, (World Scientific, 1991) 35.

[52] H. Ito, W. W. Buck and F. Gross, Phys. Lett. **B248** (1990) 28.

[53] C. Itzykson and J. Zuber, *Quantum Field Theory*, (McGraw-Hill, 1985) 482.

[54] M. R. Frank, Phys. Rev. **C51** (1995) 987.

[55] J. S. Ball and Ting-Wai Chiu, Phys. Rev. **D22** (1980) 2542.

[56] Z. Dong, H. J. Munczek and C. D. Roberts, Phys. Lett. **B333** (1994) 536.

[57] S. R. Amendolia *et al.* [NA7 Collaboration], Nucl. Phys. **B277** (1986) 168.

[58] S. R. Amendolia *et al.*, Phys. Lett. **B146** (1984) 116.

[59] D. I. Diakonov, Lectures at the Advanced Summer School on Non-Perturbative Field Theory, Peniscola, Spain, June 2-6, (1997), hep-ph/9802298.

[60] M. Creutz, *Quarks, gluons and lattices* (Cambridge University Press, Cambridge, 1983).